# Large Ocean Worlds with High-Pressure Ices

Baptiste Journaux, Klara Kalousova, Christophe Sotin, G. Tobie, Steve Vance, Joachim Saur, Olivier Bollengier, Lena Noack, Tina Rückriemen-Bez, Tim van Hoolst, et al.

**Noname manuscript No.**
(will be inserted by the editor)

# Large ocean worlds with high-pressure ices

**Baptiste Journaux · Klára Kalousová · Christophe Sotin · Gabriel Tobie · Steve Vance · Joachim Saur · Olivier Bollengier · Lena Noack · Tina Rückriemen-Bez · Tim Van Hoolst · Krista M. Soderlund · J. Michael Brown**

Received: date / Accepted: date

B. Journaux
Department of Earth and Space Sciences
University of Washington, Seattle, USA.

K. Kalousová
Charles University, Faculty of Mathematics and Physics, Department of Geophysics, Prague, Czech Republic

C. Sotin
Jet Propulsion Laboratory-California Institute of Technology, Pasadena, USA

G. Tobie
Laboratoire de Planétologie et Géodynamique, UMR-CNRS 6112, Université de Nantes, Nantes, France

S.D. Vance
NASA Jet Propulsion Laboratory-California Institute of Technology, Pasadena, USA

J. Saur
Institute of Geophysics & Meteorology, University of Cologne, Germany

O. Bollengier
Department of Earth and Space Sciences
University of Washington, Seattle, USA.

L. Noack
Freie Universität Berlin, Germany

T. Rückriemen-Bez,
TU Berlin, Berlin, Germany
DLR Institute of Planetary Research, Berlin, Germany

T. Van Hoolst
Royal Observatory of Belgium, Brussels, Belgium
Institute of Astronomy, KU Leuven, Leuven, Belgium

J. M. Brown

**Abstract** Pressures in the hydrospheres of large ocean worlds extend to ranges exceeding those in Earth deepest oceans. In this regime, dense water ices and other high-pressure phases become thermodynamically stable and can influence planetary processes at a global scale. The presence of high-pressure ices sets large icy worlds apart from other smaller water-rich worlds and complicates their study. Here we provide an overview of the unique physical states, thermodynamics, dynamic regimes, and evolution scenarios specific to large ocean worlds where high-pressure ice polymorphs form. We start by (i) describing the current state of knowledge for the interior states of large icy worlds in our solar system (i.e. Ganymede, Titan and Callisto). Then we (ii) discuss the thermodynamic and physical specifics of the relevant high–pressure materials, including ices, aqueous fluids and hydrates. While doing this we (iii) describe the current state of the art in modeling and understanding the dynamic regimes of high-pressure ice mantles. Based on these considerations we (iv) explore the different evolution scenarios for large icy worlds in our solar system. We (v) conclude by discussing the implications of what we know on chemical transport from the silicate core, extrapolation to exoplanetary candidate ocean worlds, limitations to habitability, differentiation diversity, and perspectives for future space exploration missions and experimental measurements.

**Keywords** High pressure ices · Titan · Ganymede · Callisto · Exoplanets · Habitability

## Introduction

A unique and intriguing aspect of large ocean worlds is the influence of pressure on the physical state of their hydrospheres. Pressure-induced phase transitions are well established as key features inside Earth and other planetary bodies. On larger bodies like Ganymede, Callisto, and Titan, pressures in the hydrosphere can far exceed the pressures corresponding to the bottom of Earth's deepest oceans and into the ranges of pressure encountered in Earth's lower crust and upper mantle. In this range new phases and physical properties of water appear.

High-pressure ices in Ganymede, Callisto, and Titan offer the prospect of geophysical phenomena not occurring on Earth, at least not in water. From what has been revealed by spacecraft missions—*Voyager*, *Galileo*, and *Cassini-Huygens*, mainly—these similarly sized worlds differ in composition and have likely followed drastically different thermal histories. The occurrence and geodynamic behaviors of ices II, III, V, and VI must have affected the thermal evolution of these worlds. Processes in high-pressure ices also determine the efficiency of chemical exchanges from the rocky core to the ocean, crucial to determining whether this class of planetary object may be suitable for hosting life.

Department of Earth and Space Sciences
University of Washington, Seattle, USA.

K.M. Soderlund
Institute for Geophysics
Jackson School of Geosciences
The University of Texas at Austin

The larger water-rich planetary bodies like Neptune and Uranus might also contain high pressure ices, but would not have an oceans per say, as most of their water-rich envelope is supposed to be composed of super-ionic fluids and possibly super-ionic ice XVIII at extreme pressure and temperatures conditions (33; 162; 137; 127; 126), incompatible with habitability as considered here. Therefore, these larger planetary bodies are not discussed hereafter.

This chapter covers the physical, thermodynamic, and dynamical aspects rising from the existence of thicker hydrospheres containing high-pressure ice polymorphs and other high-pressure materials, and the resulting effects of thick rocky lithospheres and iron cores in large ocean-worlds.

## 1 Existing observational constraints on Ganymede/Callisto/Titan

Here, we provide an overview of the current knowledge of the hydrosphere structures of the largest moons in our solar system. We start with the observational evidence for the presence of deep oceans and continue with the possible structures of the high-pressure ice layers.

Table 1: Properties of high-pressure ocean worlds. Moment-of-inertia values assume hydrostatic equilibrium

| | Radius (km) | Density (kg $m^{-3}$) | Moment of Inertia[d] |
|---|---|---|---|
| Titan[a] | 2574.73±0.09 | 1879.8±0.004 | 0.3438±0.0005 |
| Ganymede[b] | 2631±1.7 | 1942.0±4.8 | 0.3115±0.0028 |
| Callisto[c] | 2410.3±1.5 | 1834.4±3.4 | 0.3549±0.0042 |

[a](89; 86)
[b](155), revised from (9)
[c](7)

### 1.1 Occurrence of High-pressure Ices in the Solar System

A key difference between the small- to medium-sized moons such as Enceladus or Europa, and the large moons Titan, Ganymede, and Callisto, is a much thicker hydrosphere in the case of large moons, which results in the presence of a high-pressure ice layer between the silicate core and the deep ocean. Even though they have similar mass and radius, the large moons have different degrees of differentiation inferred from the values of the reduced moment of inertia (Table 1). As a result, for example, Titan's hydrosphere is about 500 km thick (32), much thinner than Ganymede's, which is about 800 km in thickness (183). In addition, Ganymede's surface gravity is higher than that of Titan (1.45 vs 1.35 m $s^{-2}$). Combined with the hydrosphere thickness, this creates pressures at the silicate-hydrosphere interface that are twice as high on Ganymede (1.6 GPa) as on Titan (0.8 GPa). The different pressure regimes correspond to different configurations of high–pressure ice phases depending on the assumed ocean thermal state and salinity (187) (Table 2).

As discussed below (Section 3.2), convection within the ices should proceed near the solidus temperature, leading to melt at the high-pressure ice and rock interface, and within the upper parts of the high-pressure ice (35; 95). This potentially briny liquid would have a main role in the transport of material.

### *1.1.1 Titan*

Titan's dense atmosphere and organic-rich surface hide an ice-rich crust and thick water ocean. The *Cassini* spacecraft measured high ratios of $Ar/N_2$ and $^{14}N/^{15}N$ in Titan's atmosphere relative to comet 67P/Churyumov–Gerasimenko, which has been interpreted to indicate an evolved interior source of nitrogen, most likely from organic-rich materials from Titan's interior (125). The low primordial Ar in the atmosphere has been interpreted as indicating that Titan's $N_2$ originates from $NH_3$ (138). While this finding also supports the hypothesized endogenous scenario, alternative hypotheses for the formation of Titan's $N_2$ include formation by dissociation via shock heating (122), photolysis (11), and late-stage impacts (158).

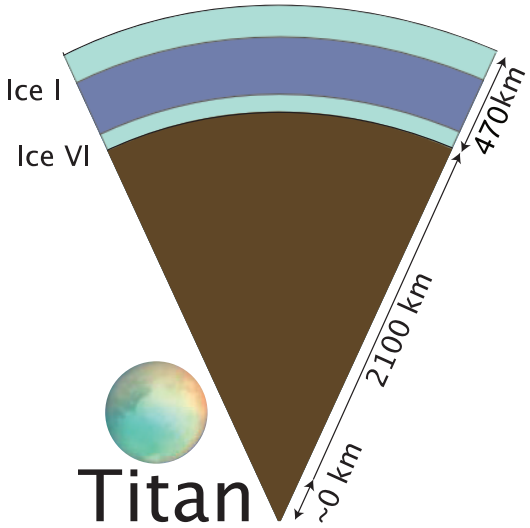


Fig. 1: Inferred internal structure for Titan, assuming the upper ice-rich crust is thinner than 100 km. Thicker ice crusts imply a colder ocean and the presence of ice V. The depths where high-pressure ices form are computed based on published values of radius, bulk density, and gravitational moments of inertia (Table 1). Such solutions are non-unique, subject to the uncertainties in bulk properties and assumptions about the composition of oceans and minerals. The required rock density in the associated models is around 2,500 kg $m^{-3}$. In previous studies (188) this low value was not achievable for the assumed silicate mineralogies. Recent work solves this problem with the addition of organic materials consistent with a CI chondrite parent body (136). Modified from (188).

The endogenous sourcing of Titan's organics implies a relation between the atmosphere's composition and the chemistry of Titan's internal liquid water ocean.

The presence of radiogenic $^{40}$Ar in Titan atmosphere suggests dissolution of K (and other ions) from the silicate core (138). An alternative model supposes that $^{40}$Ar produced inside the silicate core diffuses to the interface with HP ices, where it can be dissolved in the temperate layer and delivered to the ocean (96). Geochemical models of Titan's ocean formation, assuming efficient extraction of potassium from Titan's rocky interior (32) lead to the inference that Titan's ocean is moderately saline ($\sim$ 1Wt% aqueous NaCl) (113). Other models for Titan's ocean chemistry explore the presence of sulfates and ammonia without seeking consistency with Titan's atmospheric composition (58; 70; 187).

Titan's mean upper ice layer thickness is interpreted from *Cassini-Huygens* data to be 50-200 km, based on topography and admittance (76); less than 100 km based on shape, topography, and gravity (128); and 55-80 km based on the observed Schumann resonance (15). This entire range of thicknesses is consistent with an ice VI layer at the base of the ocean, atop a low-density silicate interior. If Titan's ice crust is indeed thin and if the ocean has a low salinity, high-pressure ices may be minimal or absent entirely.

Models of Titan's thermal evolution indicate that high-pressure ice formed in the most recent 2 Ga or even less (177).

Further analysis is needed to achieve resolve inconsistencies among the different observations of Titan's chemistry and internal structure.

### *1.1.2 Ganymede*

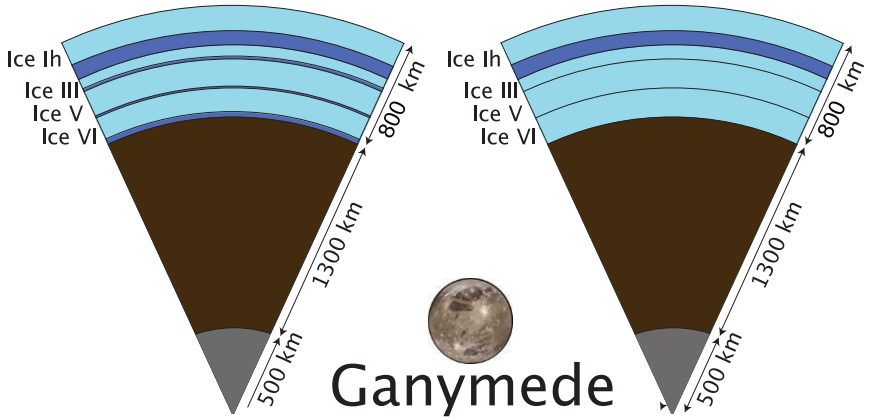


Fig. 2: Two possible internal structures for Ganymede, based on *Galileo* gravity data. Both are consistent with additional geological and geophysical constraints on bulk heat flow and on the thickness of the ice Ih lithosphere. The existence of stable liquid regions between and beneath high pressure ices (left) depends on the transport of materials within the different ices. The corresponding rock density in the associated models is around 3,500 kg m$^{-3}$, and the assumed Fe core density (including 20 wt% S as FeS) is 7,200 kg m$^{-3}$. Modified from (188).

Ganymede's intrinsic magnetic field and small normalized moment of inertia suggest that it experienced enough heating for a liquid iron core to differentiate from the silicate mantle. Convection in the ice crust is in accord with the formation

of grooved terrains on the surface (73) that are much younger that the heavily cratered terrains. The thickness of the hydrosphere probably exceeds 800 km (188). Ice III forms at the base of the ocean (Table 2) and atop ices V and VI for a cold model Ganymede ($\approx$ 1 $mW^{-2}$ at the surface) with a high-salinity ocean containing 10 wt% of $MgSO_4$ (Fig. 2). However, this ice is buoyant relative to the model ocean; such upward snowing ice would seem to be dynamically short-lived, perhaps hastening the cooling of Ganymede and thickening the ice I crust such that ice III accumulates underneath the ice I and the ocean interface. Warmer oceans within the likely limits of Ganymede's heat (20) can eliminate ices III and V, but even just after its formation Ganymede seems likely to have had some amount of ice V.

The role of ocean salinity is key in determining which high-pressure ices form, and their dynamic stability. It has been established in recent years that briny fluids under pressure can have densities exceeding those of high-pressure ices (80; 92; 183) and might reside stably between the different layers of high-pressure ice (93; 184). The left-most schematic in Fig. 2 illustrates a scenario with dense salty fluids between high-pressure ices. Such a scenario is plausible thermodynamically, but the stability of salty fluids under the ices requires detailed geodynamic modeling of the type performed in recent years for pure-water oceans (e.g., 95).

The presence of solid ions in high-pressure ices may also have significant effects on their thermal evolution and geodynamics. Dissolved ions incorporate into ice VI (and possibly also in ice phases II, III, and V). The incorporation of salt in ice VI, based on studies of rubidium iodide, is three times that in ice Ih (93).

Ganymede's HP ice layer may lie upon a dry silicate mantle that still contains a significant amounts of insoluble organic matter (IOM), as recently proposed by (141) in order to reconcile the measured mass and moment of inertia with the equations of state (EoS) of $H_2O$ and silicates.

### *1.1.3 Callisto*

The evidence for an ocean at Callisto is not as strong as the evidence for oceans in Ganymede and Titan. Callisto's bulk MoI is larger than that of Titan (Table 1) suggesting an even less differentiated interior (7) and a thinner hydrosphere. The value of the MoI (Table 1) assumes hydrostatic equilibrium. If this assumption is not verified by future missions such as ESA's *JUICE* mission, then the error on the MoI could be very large (65) and Callisto may be more differentiated than presently thought.

The poor constraints on Callisto's density structure mean that an ocean there could be less than 250 km deep (Fig. 3), with little or no high-pressure ice. Or it could be more like Titan, with a seafloor at pressures approaching 800 MPa covered in ices V and VI (Table 2). The heavily cratered surface surface suggests weak or no differentiation; if Callisto has differentiated, it is difficult to conceive of how it would have cooled within a few hundred Myr to retain its cratering record. In either case, the fully stagnant upper lithosphere (124) suggests the ocean is nearly frozen and so has a near-eutectic composition. Buoyant ice II or III may be present, unless the ocean contains strong freezing suppressants such as ammonia or methanol.

Because of the greater uncertainties in the characteristics of Callisto's hydrosphere and the likelihood that Callisto has experienced less heating than Ganymede,

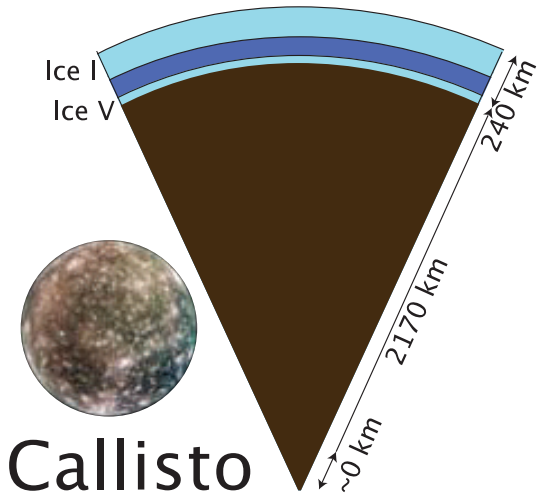


Fig. 3: Inferred internal structure for Callisto. The corresponding rock density in the associated models is around 3,000 kg $m^{-3}$. Modified from (188).

most studies of the dynamics of HP ice layers have focused on Ganymede and Titan.

## 2 High-pressure physical chemistry of ices, aqueous solutions and relevant solids

As described in the previous section, the pressures and temperatures expected in the hydrospheres of large icy moons (200–400 K and 0–1.6 GPa) extend into the domain of stability of several high–pressure ice polymorphs, aqueous solutions of varying compositions, and possibly other solid phases (mostly hydrates) of neutral volatiles (gases) and ionic species (salts). Each of these phases has a different structure and sometimes contrasting thermophysical properties. Consequently, comprehensive studies of the hydrospheres of water-rich planetary bodies remain challenging tasks requiring accurate accounts of the pressure, temperature, and chemical (PTX) dependencies of the properties of these phases. These properties can be classified as equilibrium thermodynamic properties (e.g., density, heat capacity, thermal expansivity, entropy, chemical potential) and transport properties (e.g., thermal diffusivity, viscosity, electrical conductivity). Equilibrium properties can be directly derived from representations of thermodynamic potentials such as the Gibbs or Helmholtz free energies. Such equations of state (EoS) can be determined from experimental data or first-principle calculations (e.g., density functional theory, molecular dynamic modeling). Transport properties are not directly derivable from Gibbs-energy and therefore need to be determined in-situ or from calculations, which are both challenging in the relevant range of PT conditions. This section aims to provide an overview of the known PTX dependencies of important physical properties of the relevant ice polymorphs, aqueous solutions and other solids found in the hydrosphere of ocean-worlds. A look-up table of

high-pressure ices and liquid water properties at relevant ocean-worlds conditions is provided at the end (Table 2).

## 2.1 Water phase diagram at high-pressure

The water phase diagram, and more particularly its solid phases, has been a rich topic of research since the discovery and description of its polymorphism in the beginning of the 20th century by Bridgman (1912) (25). To date, 18 crystalline polymorphs have been characterized experimentally (126), and about three orders of magnitude more were explored recently through first principle calculations (49). Many of these ice structures are stable or metastable above room pressure in a dense configuration (i.e., with a higher density than liquid $H_2O$ along their melting curves). A complex collection of amorphous water ices also exists with many metastable forms. One of phases, high-density glassy water (HDG), which forms by vapor deposition and irradiation, could be a major phase at the surface of water-rich objects (145; 66). The more complex region of the phase diagram is arguably between 1 and 20.000 bar (0.1 to 2000 MPa) below room temperature, where most of the polymorphs have been found (i.e. Ih, *Ic, II, III, *IV, V, VI, *IX, XI, *XII, *XIII, *XIV and XV; metastable phases noted with an asterisk) as well as a suite of clathrate hydrate structures (with various host molecules). This PT range is of particular relevance regarding the hydrospheres of icy moons, since much higher pressures (and temperatures) may be found inside water-rich exoplanets. While metastable phases may exist in natural environments (e.g., ice Ic on Earth), stable phases are considered more likely to play a significant role in the structure of high-pressure water-rich mantles. This section therefore focuses mainly on the stable ice phases Ih, II, III, V, VI for icy moons, and to some extent to VII and X for water-rich exoplanets.

Figure 4 displays the stability fields of the stable water ice polymorphs and some relevant clathrate hydrates up to 3 GPa, in the temperature range of interest to the hydrospheres of water-rich planetary bodies. Above that pressure, cubic ice VII – and its possible variants $VII_t$, VII' and VI"– remains stable to high pressures, with a gradual second order transition to ionic ice X above 50-100 GPa (77) and super-ionic ices above 2000 K (126).

## 2.2 Aqueous solutions at high-pressure.

### *2.2.1 Equilibrium thermodynamic properties*

The physical and thermodynamic properties of aqueous solutions over this large range of pressures and temperatures remain active topics of research. Some studies have focused on pure water liquid-ice equilibria relevant to the study of icy ocean worlds (37; 38; 42). While this approach has led to a description of the melting curves up to the ice VII domain (37; 38), the fragmentary measurement results and limited computational constraints available for ices have limited progress, especially at lower temperatures and higher pressures. Ideally, independent equations of state at the level of complexity required to describe accurately the behavior of

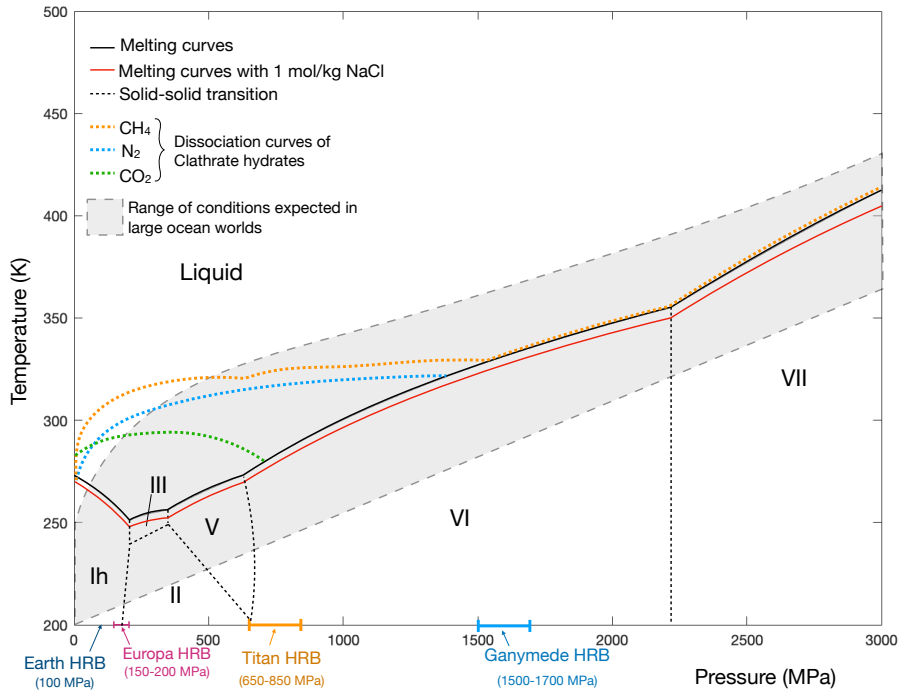


Fig. 4: Phase diagram of water showing stable ice polymorphs relevant to water-rich planetary body interiors. Melting curves and solid-solid phase transitions up to ice VI are from Journaux et al. (2020) (90). Ice VII melting line is from Wagner et al. (2011) (190), and ice VI-VII solid-solid phase from experimental data by Bridgman (1937) (26). The grey shaded area correspond the the approximate range of conditions expected in ocean worlds. Clathrate hydrate dissociation curves are approximated from experimental data discussed in Sohl et al. (2010) (163) and completed for $CO_2$ in Bollengier et al. (2013) (22). The pressure range of the hydrosphere-rock boundary (HRB) is also reported for Earth, Europa, Titan and Ganymede.

each phase of interest (and properly constrained by measurements) should provide predictions matching known phase equilibria as well as the thermodynamic properties inside and outside the range of stability. Here we use the SeaFreeze software framework, which offers a self-consistent description of high-pressure ice polymorphs and liquid water up to 2300 MPa (90; 21). Historically, the most commonly used thermodynamic representation for properties of fluid water remains the IAPWS-95 formulation (189), an equation of state parameterize to reproduce thermodynamic data to 1 GPa and 1273 K (with a fair extrapolation capability to 100 GPa) (189). While IAPWS-95 extends to the gaseous and supercritical domains of water, limited data above 100 MPa (particularly below 273 K) at the time of its release limited its accuracy near melting temperatures; uncertainties near the melting curve of ice III reach 0.2% for the density, 0.3% for the speed of sound, and 20% for the specific heat (21). Since the release of IAPWS-95, improved measurements of thermodynamic properties, particularly of sound speeds, motivated the publication of updated equations of state up to 0.4 GPa (81) and 2.3 GPa (21). The adoption of representations of thermodynamic potentials (here

the Gibbs energy) based on polynomial local basis functions gives access to equilibrium thermodynamic properties (e.g. density $\rho$, heat capacities $C_P$ & $C_V$, bulk moduli $K_T$ & $K_S$, thermal expansivity $\alpha$, chemical potentials $\mu$, sound speed, entropy $S$ and enthalpy $H$) as simple analytic functions obtained from the derivation of the reference potential. Furthermore, such a framework brings flexibility in the incorporation of new data sets within the domain of the representation (to update the equation of state), and allows the domain of the representation to be extended without impact in the initial domain (27).

Figure 5 illustrates the variation in thermodynamic properties ($\rho$, $\alpha$, $C_P$,$K_T$ and sound speed) for pure water (21) and 1 mol·kg$^{-1}$ NaCl(aq) at 270, 300 and 35 K, computed using SeaFreeze (90) and an aqueous NaCl Gibbs parameterization under development, based on Brillouin data (119) and new ultrasonic measurments using the same methodology as in (21). As is apparent in the figure, pressure has the largest overall effect on the properties of aqueous solutions, and its consideration becomes critical at the scale of massive hydrospheres. Temperature has a strong visible effect on density, thermal expansivity and heat capacity, but its impact on bulk modulus and sound speed remains limited.

Quantifying the effects of chemistry at high pressures remains a more challenging endeavor as solvation interactions (and therefore their resulting effects on thermodynamic properties of solutions) strongly depend on the solute species and the pressure and temperature conditions. Therefore, one needs to experimentally measure these properties in-situ. Expected main planetary solutes include ionic species such as NaCl, $MgSO_4$, and $Na_2SO_4$; as well as organics such as $NH_3$, $CH_4$, and $CO_2$ (197; 163). In figure 4 we only display the effect of 1 mol·kg$^{-1}$ of dissolved NaCl (approximately twice the sea-water concentration) for clarity, but other species, and ternary mixtures, will be included in the SeaFreeze framework (e.g. $MgSO_4$, $Na_2SO_4$, $MgCl_2$, $NH_3$ and $CO_2$). Aside from this work, scarce thermodynamic data and modeles currently exist for the pressure range found in large ocean worlds.

Thermodynamic representations based on experimental data exist for ammonia up to 2.3 GPa (including HP ice equilibria) (38) and for $MgSO_4$ (184; 183). For other ionic species, simple binaries of the Na-Mg-Cl-$SO_4$ system have been extensively studied below 100 MPa (the domain of Earth's oceanic pressures), but higher pressures and more complex mixtures remain largely unconstrained to this day (60; 163; 183; 188). For NaCl(aq), the results presented in Figure 5 are from the SeaFreeze Gibbs-energy representation, based on preliminary sound speed measurements under final development (Fig. 5) [see Bollengier et al. (2019) (21) for a description of the initial laboratory measurements on pure water]. The largest effects of chemistry change are visible for the density, thermal expansivity and heat capacities, with a lesser influence on the bulk moduli and the speed of sound.

As reported in the previous section of this chapter, concentrated brines can become denser than some high-pressure ices (80; 92; 183), potentially creating intermediate melt pockets at ice-ice interfaces or at the hydrosphere-rock boundary (92; 183). It should be noted that the concentrations required for density inversion to happen are generally above 1-1.5 mol/kg (depending on the solute molar mass and the density of the ice polymorph). Such concentrations exceed those expected from the inferred bulk compositions of icy moons in the solar system (197). Where density inversions occur, they may create localized reservoirs of dense brines under

high-pressure ice, rather than global density inversions that decouple the high-pressure ice from the solid layer below it.

#### *2.2.2 Transport properties*

Published measurements of the physical transport properties of aqueous solutions at high pressures, including electrical and thermal conductivities, are limited above 100 MPa. Some of the recent work and possible extrapolation to cover the range of icy worlds interiors is reviewed in Vance et al. (2018) (188). Some general considerations are given hereafter based on the available data. These should be regarded as indicative and subject to discussion depending on the solutes of interest, since the effects of high pressure on solution properties remain poorly understood.

The electrical conductivity of brines can vary over several orders of magnitude depending on the solutes concentration, as illustrated by the difference between pure water ($< 10^{-5}$ S/m) and seawater ($\simeq$5 S/m). Increasing pressure or decreasing temperature usually decrease electrical conductivity, as seen for $MgSO_4$ brines (111). Similar trends are observed for seawater (82) and NaCl brines up to 400 MPa (4; 79).

The thermal conductivity of NaCl brines seems to follow the overall trend of pure water as a function of temperature, with a peak around 680 mW/(m K) at 140 K (5). Increasing NaCl(aq) concentrations decrease thermal conductivity by 1-3% per molal of NaCl depending on the pressure and temperature range. Increasing pressure will decrease the thermal conductivity by roughly 1-3% per molal as well depending on the temperature range. The model by Aleksandrov et al. (2013) (5) only covers the 0-100 MPa range, making the extrapolation to higher pressures uncertain.

### 2.3 High-pressure ice polymorphs

High-pressure ice polymorphs have different crystallographic structures, leading to contrasted thermodynamic and transport properties (see section on viscosities hereafter). The first discovery of ice polymorphism was reported by (174)and then further-explored by (25; 26). The pure water melting curves and solid-solid phase transitions (see Figure 4) remain, to this day, mainly constrained by these old datasets (37; 42; 191).

#### *2.3.1 Equilibrium thermodynamic properties of ice polymorphs*

The gold standard for the ice Ih equation of state is currently the Feistel and Wagner (2006) parameterization (56) that provides a way to derive all important equilibrium thermodynamic properties from pressure and temperature derivatives of the Gibbs potential. High-pressure ices have remained sparsely studied until recently as they were only of interest to the physical chemistry community.

Melting curves and triple points of pure compounds are usually described by Simon curves. Parameterizations of this kind have been derived for all the ices by Choukroun and Grasset (2007) (37) and Wagner et al. (2011) (191).

Recent pressure-volume-temperature measurements by Journaux et al. (2020)(90) have enabled a full Gibbs energy representation for ices III, V and VI. Figure 6

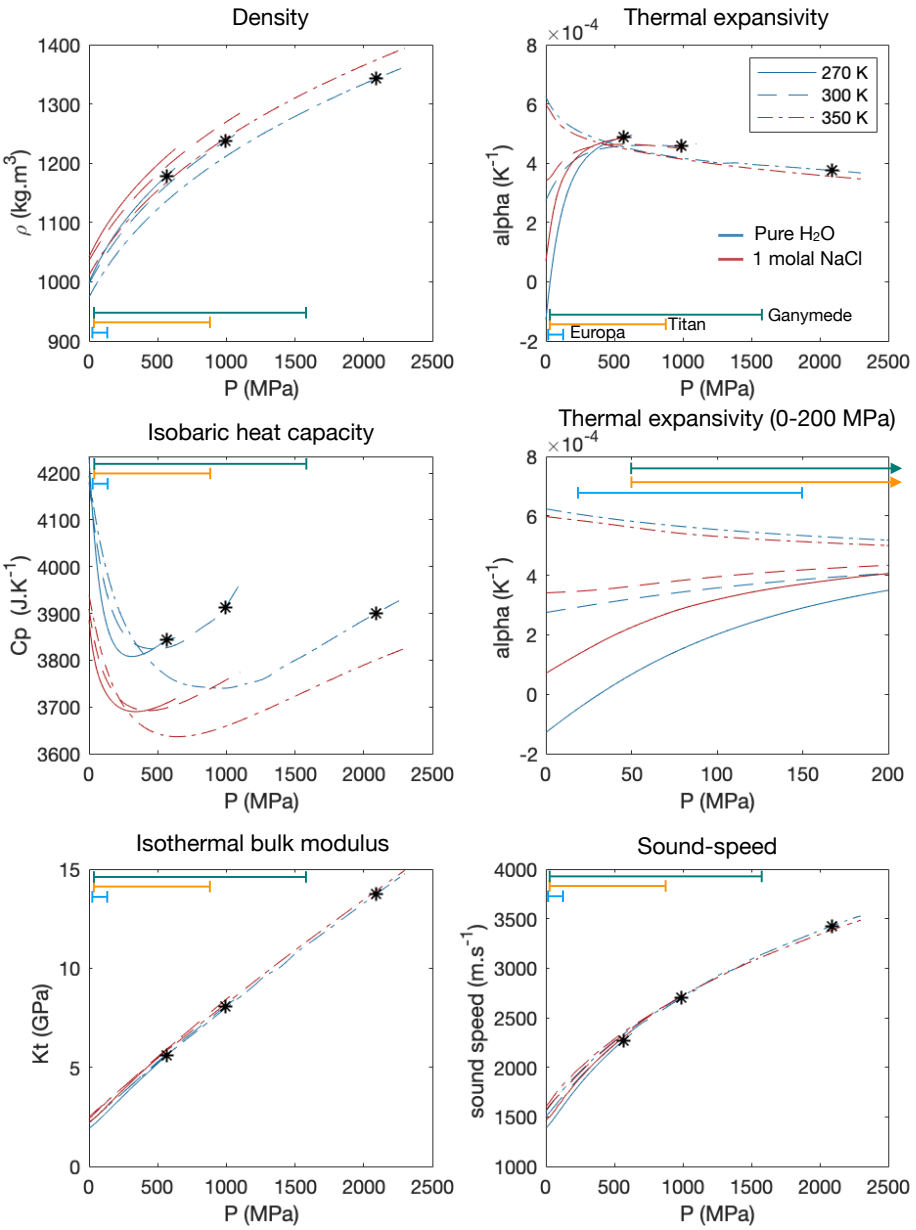


Fig. 5: Aqueous solutions (pure $H_2O$ and 1 mol·kg$^{-1}$ NaCl) equilibrium thermodynamic properties versus pressure at 270, 300 and 350 K computed with the SeaFreeze framework (90). Dark asterisks represent high-pressure ice freezing temperatures, with ice V freezing at 270 K and ice VI at 300 and 350 K. The estimated pressure range of icy moon hydrospheres are reported for Europa, Titan and Ganymede.

illustrates the evolution with pressure of the main equilibrium thermodynamic properties (density, thermal expansivity, heat capacity and isothermal bulk modulus) and seismic wave velocities, from 250 to 300 K, computed using the SeaFreeze package. Phase transitions and pressure variations have a significant influence for all thermodynamic parameters and seismic wave velocities shown here. The relatively small temperature range of interest for planetary hydrospheres (250-300K) has an important effect on the thermal expansivity and heat capacity of all polymorphs. The density, bulk modulus, and seismic wave velocities remain mainly influenced by pressure and phase transitions. Ice II is not represented here for clarity as its stability range lies <250 K, thus making it less relevant for hydrospheres interior. Details on its properties can be found in (188; 90).

It is also worth discussing the effect of chemistry on high pressure ices. Ice VI is the only high-pressure polymorph with ice VII to have been investigated for salt incorporation (RbI as a NaCl analogue) (93). Ice VI seems to behave in a similar manner to ice Ih by mostly rejecting salts out of its structure during growth at equilibrium with a partition coefficient $K_d(RbI)$ close to $5{\cdot}10^{-3}$ (93). Nonetheless, the very small amounts incorporated can have a significant effect on lowering its density (93). The extent to which other planetary solute species (e.g. $MgSO_4$, $MgCl_2$, $Na_2SO_4$, etc.) incorporate into high–pressure ices still remains unconstrained to this day.

Ice VII has been the most studied after ice Ih, due to its large stability field over 2 GPa and 300 K. This pressure is beyond the current conditions found in any icy worlds in the solar system. It should be present in larger ocean super-Earth exoplanets (167; 93; 139). Ice VII is a more complex phase, as it seems to have several states of proton ordering (77) and is able to incorporate large amounts of ionic species while retaining its structure ($K_d(RbI) = 0.12$) (105; 93; 23). Many pressure-volume-temperature data points and equations of state (EoS) are available for the pure $H_2O$. The most recent and common in the planetary science literature for ice VII up to 50 GPa and below 1000 K are from (18) and (106). For pressures above 50 GPa and temperature above 1000 K, in the range interesting for ocean exoplanets, the evolution of thermodynamic properties and the location of phase transitions into plastic phase, ice X or super-ionic ice, remains an active field of experimental and theoretical study (62; 77; 126).

### *2.3.2 Thermal and electrical conductivities of water ice polymorphs*

Thermal conductivities of ice polymorphs have been measured experimentally by Andersson et al. (2005) (10). They all lie in the 1-6 W/(m K) range for ice III, V, VI, II and Ih, in increasing order of thermal conductivity. Ices generally have higher thermal conductivities than aqueous solutions (as described above) and clathrate hydrates (as described below).

The electrical conductivities of ices generally obey the Jaccard model, in which protons are the charge carriers (88; 57). Increasing pressure, temperature, close packing of the lattice structure, and static or dynamic proton disorder can ease significantly the propagation of defects and the diffusivity of protons, resulting in larger electrical conductivities. Overall, ice polymorphs are not good electrical conductors, with electrical conductivity $<10^{-5}$ S/m for ice Ih (57), $<10^{-4}$ S/m for ice VI and $<10^{-3}$ S/m for ice VII (143; 115). Electrical conductivity of ice II, III and V remain unconstrained to this day. Except for proton-ordered ice II, disorderd

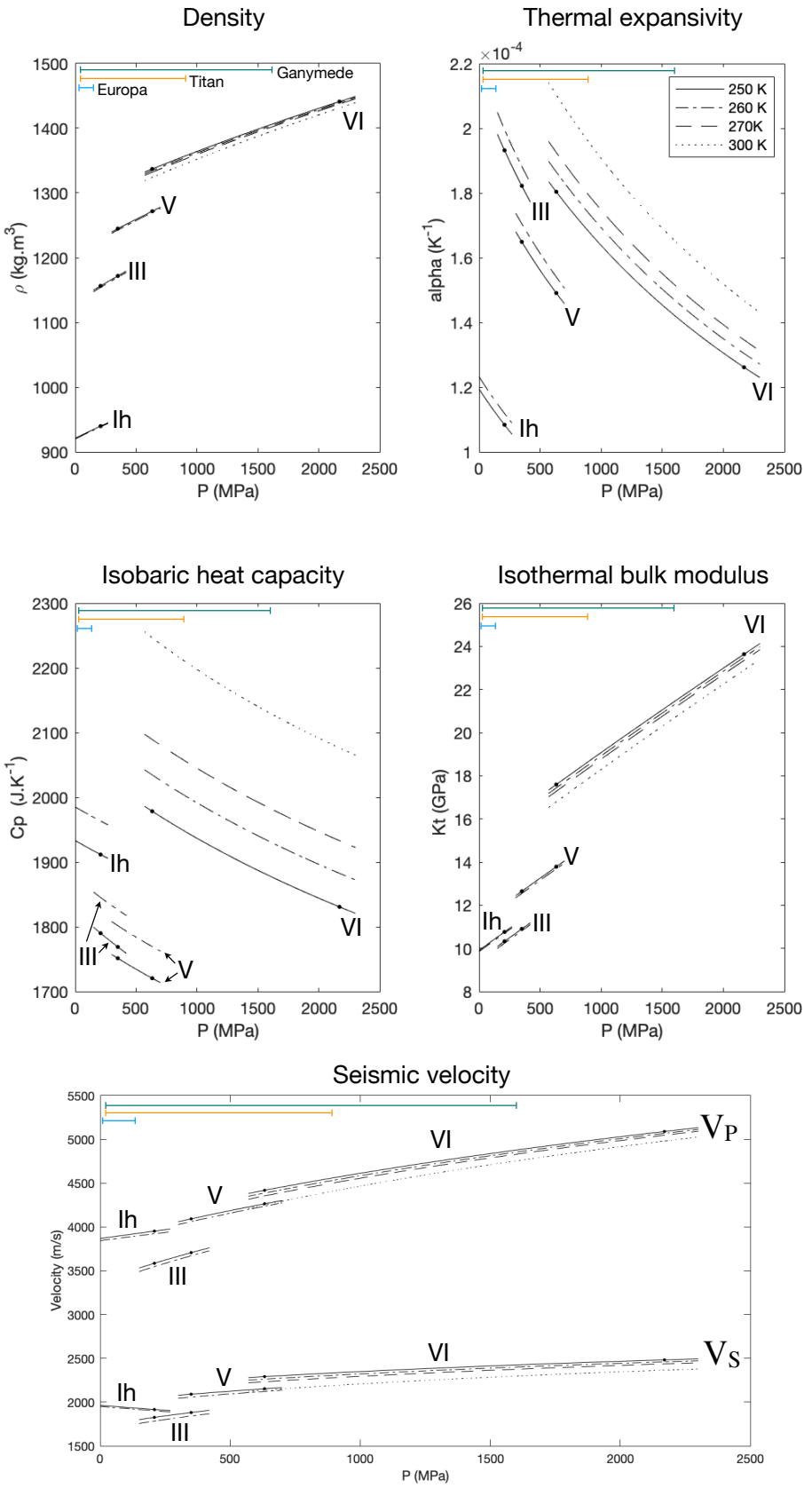


Fig. 6: Ice polymorphs thermodynamic properties and seismic velocities evolution with pressure extracted from the SeaFreeze framework (90) at 250 and 260K for ices Ih, III, V, VI and 270 and 300K for ice VI only. Black dots show the position of the solid-solid phase transition.

ice III and V should have similar proton dynamics to ice Ih or VI and therefore should have electrical conductivities in between those of the latter. Transition to super-ionic ice is observed above 100 GPa and 2000 K, when proton diffusivity increases significantly, results in a major increase in electrical conductivity to $10^2$ S/m - $10^3$ S/m (127).

## 2.4 Other relevant solids for ocean world hydrospheres

Because of the likely presence in extraterrestrial hydrospheres of many ionic (e.g. NaCl, $Na_2SO_4$, $MgSO_4$, $MgCl_2$) and volatile species (e.g. $CH_4$, $NH_3$, $CO_2$), other water-bearing solid phases may be expected to contribute to the internal structures and geophysical processes of icy worlds.

### *2.4.1 Clathrate hydrates*

Clathrate hydrates comprise a family of water-rich compounds in which a skeleton of hydrogen-bonded $H_2O$ molecules forms cage-like structures that trap usually neutral guest molecules (e.g. $CH_4$, $N_2$, $CO_2$). Generally, no bond between the host and guest species occurs; rather, van der Waals interactions between the guest and the surrounding water molecules stabilize the structure itself. The thermodynamically favored combination of cage type, or clathrate structure (i.e. CS-I, CS-II, SH, sT, FIS), changes depending on the PT conditions and the nature of the guest species. Several species may occupy a single structure simultaneously. Some properties of clathrate hydrates are similar to that of water ices: for example, the thermal expansion, heat capacity and elasticity of the CS-I and CS-II structures are close to that of ice Ih (39). However, due to their nature, clathrate hydrates exhibit distinct values of thermal conductivity, viscosity and density.

As illustrated in Figure 4, clathrate hydrates may become more stable than water ices between a few MPa and up to GPa pressures (see reviews by (163) and (39)). However, this stability is dependent on the abundance of the guest species in the environment, controlled by the partial pressure of the guest species but limited by their solubility in water. In the absence of guest molecules, the empty cages remain highly unstable but can be observed at cryogenic temperatures, as was successfully demonstrated for an emptied CS-II structure (52) (see also the comparable achievement for a higher-pressure"filled ice" by (150)). Because of this compositional variability, clathrate hydrates may be considered as solid solutions. A successful approach in the thermodynamic modelling of clathrate hydrates has been to consider the empty water structure as a reference state stabilized by the statistical filling of the cages by the guest molecules. The thermodynamic modeling of these phases thus remains challenging at higher pressures where the activity and solubility of many gases of interest to planetary science is poorly constrained, particularly at lower temperatures. Reviews of the different clathrate structures, guest molecules and thermodynamic modeling are provided by (94) and (39).

The specific thermophysical and rheological properties of clathrate hydrates have important consequences for the structure and processes of icy worlds. Densities vary largely, depending on the structure, occupancy, and type of guest species. Clathrate hydrates of lighter volatiles like $N_2$, $CH_4$, or $CO_2$, while generally less dense than HP ices, can achieve buoyancy or sink in aqueous solutions depending

on the pressure, temperature, clathrate structure, and aqueous composition. As for thermal conductivity and rheology, the methane CS-I clathrate hydrate has thermal conductivity up to one order of magnitude smaller, and viscosity one order of magnitude larger, than ice Ih (192; 46). These combined factors potentially make clathrate hydrates mechanically stiffer thermal insulators at the ice-ocean interface (98). The thermophysical and rheological properties of other clathrate hydrate structures (CS-II, SH, sT, FIS) remain poorly constrained at higher pressures.

In summary, because of their unique properties, clathrate hydrates of common planetary volatiles are expected to play an important role in the dynamics, chemical layering, thermal states and geological histories of planetary hydrospheres.

### *2.4.2 Other hydrates*

Most volatiles of planetary interest adopt clathrate structures under increasing pressure (39). Even if their total mass fraction in large icy moons is small, they may have a strong influence of on the thermal and compositional evolution.

$N_2$, $CH_4$, Ar and Kr adopt two to three different clathrate hydrate structures between 0 and 1∼2 GPa. Above this pressure, these structures give way to a different type of higher-pressure hydrate called "filled ice". These phases abandon the cage-like skeletons for configurations more similar to the known water ice phases—for example ice Ih—with larger quantities of guest molecules stored in the channels formed by the water molecules. $CO_2$ presents a more singular case, as a single clathrate hydrate structure destabilizes into a filled iced structure below 1 GPa(6; 121), and into a mixture of $H_2O$ and $CO_2$ ice above 1 GPa (78; 22). Above 3∼4 GPa however, a change of speciation of $CO_2$ leads to greater solubility of C and the appearance of crystalline, hydrated carbonic acid (193; 1; 2).

Other types of hydrates of relevant molecules can form at the pressures and temperatures found inside planetary hydrospheres. Many salt hydrates have already been identified at ambient pressure, with as many as 11 so far for $MgSO_4$ alone (with meridianiite, $MgSO_4{\cdot}11H_2O$, the hydrate stable at the eutectic at 0.1 MPa) (36); several transitions to new $MgSO_4$ hydrates have been reported at GPa pressures (72). For NaCl, the eutectic phase transits from hydrohalite at 0.1 MPa to halite at 1200 MPa (3). Many other phases of salts hydrates remain to be discovered at high pressure for single salt-water systems, and even at 0.1 MPa for mixtures of salts, as suggested by experiments on $H_2O$-NaCl (181) and $H_2O$-$MgSO_4$ (135) systems.

Ammonia has the ability to form hydrogen bonds with water, thus facilitating the stability of several hydrates structures. A large diversity of ammonia hydrates phases have been identified (but not all characterized) with three known stoichiometric mixtures: ammonia dihydrate (ADH, $NH_3{\cdot}2H_2O$), ammonia monohydrate (AMH; $NH_3{\cdot}H_2O$) and ammonia hemihydrate (AHH; $2NH_3{\cdot}H_2O$). Every mixture has a complex phase diagram at high pressures, with four known phases for ADH (61), six for AMH (116), and 2 experimentally confirmed but up to potentially 5 for AHH (148).

### 2.5 Look-up table with main properties

The following table provides a summary of high-pressure ices and liquid water thermodynamic properties and seismic wave velocities at typical conditions of ocean worlds in our solar system. All values were computed with the SeaFreeze framework (90).

| **Typical conditions** | P (MPa) | T (K) | Phase | $\rho$ (kg/m$^3$) | $\alpha$ (K$^{-1}$) | Cp (J/kg) | Cv (J/kg) | Kt (MPa) | Vp (m/s) | Vs (m/s) | Ref |
|---|---|---|---|---|---|---|---|---|---|---|---|
| Icy moon surfaces | 0 | 100 | ice Ih | 933 | 3.04E-05 | 874 | 873 | 10445 | 4183 | 2172 | (56) |
| Icy moon ocean ceilings | 50 | 260 | liquid | 1024 | -7.08E-05 | 4028 | 4025 | 2021 | 1405 | - | (21) |
| **Bottom ocean** | | | | | | | | | | | |
| Europa | 150 | 270 | liquid | 1066 | 2.90E-04 | 3856 | 3794 | 2875 | 1656 | - | (21) |
| Callisto | 300 | 250 | liquid | 1124 | 4.05E-4 | 3615 | 3478 | 3734 | 1859 | - | (21) |
| Titan | 400 | 260 | liquid | 1146 | 4.60E-04 | 3743 | 3528 | 4493 | 2040 | - | (21) |
| Ganymede | 600 | 270 | liquid | 1186 | 4.92E-04 | 3847 | 3526 | 5808 | 2311 | - | (21) |
| **Top HP ices** | | | | | | | | | | | |
| Ganymede | 300 | 250 | ice III | 1166 | 2.07E-04 | 1814 | 1725 | 9761 | 3665 | 1863 | (90) |
| Callisto | 400 | 260 | ice V | 1248 | 1.78E-04 | 1805 | 1719 | 13134 | 4094 | 2070 | (90) |
| Titan | 600 | 270 | ice VI | 1326 | 2.43E-04 | 2149 | 1971 | 14822 | 4335 | 2226 | (90) |
| **Bottom HP ice** | | | | | | | | | | | |
| Titan/Callisto | 800 | 280 | ice VI | 1341 | 2.30E-04 | 2168 | 1993 | 15877 | 4419 | 2233 | (90) |
| Ganymede | 1600 | 300 | ice VI | 1396 | 1.82E-04 | 2151 | 2007 | 20273 | 4755 | 2298 | (90) |
| **General HP ices in their stability field** | | | | | | | | | | | |
| ice III | 250 | 250 | ice III | 1160 | 2.14E-04 | 1824 | 1730 | 997 | 3622 | 1843 | (90) |
| ice V | 500 | 250 | ice V | 1260 | 1.63E-04 | 1741 | 1667 | 13890 | 4187 | 2125 | (90) |
| ice VI | 900 | 260 | ice VI | 1355 | 2.04E-04 | 2035 | 1899 | 17022 | 4535 | 2307 | (90) |

Table 2: Thermodynamic properties of ice polymorphs and liquid water at pressure and temperature conditions relevant to ocean worlds. Inferred conditions are based on the *PlanetProfile* interior models from (188).

## 3 Dynamics of HP ice layer and exchange processes

In large ocean worlds, the presence of a thick HP ice layer prevents direct contact between the ocean and the silicate mantle. However, the exchange of materials between these two layers might still be possible via convective flow in the HP ices. In addition to facilitating the transfer of materials, the dynamics of the HP ice layer also govern the extraction of heat from the deep interior. Understanding these dynamics is thus crucial for addressing the habitability of large ocean worlds. In the following, we first summarize what is known about the HP ice viscosity because it controls the layer dynamics. We then proceed to describe the current state of knowledge of the dynamics of the HP ice layers of Ganymede and Titan. To our knowledge, no such study has been performed for Callisto.

### 3.1 HP ice viscosity

Viscosity, the ratio of shear stress to strain rate, is a critical parameter that controls dynamics of the HP ice layer. For the very differentiated Ganymede that has a thick hydrosphere, the main HP ice phase is ice VI, while for Titan, which is less differentiated and has a thinner HP ice layer, both ice VI and ice V should

be considered. Ices III and II may also occur if the oceans are sufficiently cold, as discussed below. Assessing the viscosity of HP ice phases is critical for anticipating the dynamics of HP ice mantles.

The viscosity of HP ices has been measured by two groups. Sotin et al. (166) measured the deformation of ice VI at large values of shear stress (light blue rectangle in Figure 7) and found deformation rates of $10^{-2}$ $s^{-1}$ (viscosity of $10^{10}$ Pa s, blue dots). They also found a small value of the stress exponent, which is interpreted as resulting from the experimental temperature being close to the melting temperature. Extrapolation of their results to typical convective shear stresses (gray rectangle) gives viscosities on the order of $10^{12}$ to $10^{14}$ Pa s, similar to the viscosities of ice I at its melting point, which are also very close to field measurements on glaciers (yellow rectangle) (84).

Another group, led by Durham (45), measured the viscosity of ice VI at smaller values of confining pressure (light red rectangle in Figure 7) and found stronger stress dependence (i.e., larger values of the stress exponent) (red dots). Extrapolation of their measurements to typical convective stresses suggests melting point viscosity on the order of $10^{17}$ to $10^{23}$ Pa s, which is orders of magnitude larger than values extrapolated from (166). Both studies (166; 45) suggest that viscosity is close to constant along the melting curve, which justifies the use of an Arrhenius law (35; 95). Extrapolation from laboratory experiments (high stresses) to natural conditions (small stresses) can add large uncertainties, so numerical simulations usually consider a large range of viscosity values (35; 95; 96).

The relative viscosity of ice V compared to ice VI can be determined at the transition between the two phases. Figure 7 also shows the values of ice V viscosity (lines) at the triple point ice V-ice VI-water. Sotin and Poirier (169) (blue lines) observed that ice V is harder to deform than ice VI and that their viscosity ratio is close to two orders of magnitude at the experimental conditions. By contrast, Durham et al. (45) found that ice V and ice VI deform in a similar manner.

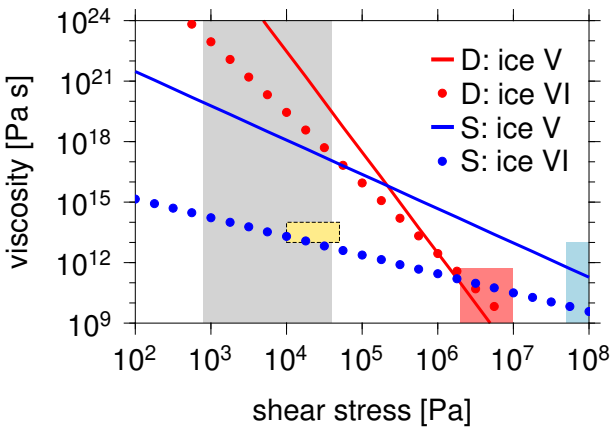


Fig. 7: Viscosity of ice VI (dots) and ice V (lines) as a function of shear stress measured by (166; 169) (blue) and (45) (red). Light blue and light red rectangles indicate the experimental conditions. Grey rectangles indicate the range of convective stresses, and yellow rectangles show the range of viscosities measured in terrestrial glaciers (84).

Ice II and III can also be stable in the interior of large moons under certain pressure-temperature conditions (cf. Section 1.1). At laboratory conditions, ice II is the strongest among all ice phases while III is the weakest (43). Both phases also exhibit at least one change in deformation mechanism. Extrapolation to lower stresses appropriate for the icy moons interiors does not significantly modify the relative strength of these two phases. The strong viscosity contrast between ices I, II (much stronger) and III (much weaker) may lead to layering and disruption of the large scale convection pattern (44).

### 3.2 Dynamics and exchange processes through the HP ice layers

The HP ice layer is squeezed between the silicate core and the ocean and is likely to be convecting according to the values of viscosity described previously. The presence of the above lying ocean implies that there is no cold thermal boundary layer (the temperature close to the ocean follows the melting curve) and thus the dynamics is driven by the upwelling thermal and compositional plumes that form at the bottom boundary.

The thermal-chemical evolution of the whole hydrosphere, including the HP ice layer, has been investigated by several authors for both Ganymede and Titan (102; 69; 161; 176; 58; 71; 20). In the majority of these studies, heat transfer through the HP ice layer was not explicitly treated and the temperature profile within the HP ice was assumed to follow the melting curve. Another approach is to describe the thermal state and heat transfer of the HP ice layer using scaling laws based on the instability of a hot thermal boundary layer at the interface with the silicates - this strategy was adopted by (71) for Titan and (139) for water-rich exoplanets.

To infer the effect of transitions between the different ice phases on convection in large satellites, (16) performed a linear stability analysis considering a model consisting of two layers with the same viscosity and thickness. They found that an exothermic phase change can either impede or enhance the whole-layer convection, depending on the ice viscosity. For endothermic transitions, they showed that phase change always inhibits whole-layer convective overturn and tends to enforce two-layer convection. A study extending their approach (168) found that taking into account different thickness and viscosity results in whole-layer convection for a much larger range of phase transition parameters than previously thought.

Recently, Choblet et al. (35) performed numerical simulations of convection in the HP ice layer in 3D spherical geometry. They showed that melting can occur in the HP ice layer for a wide range of model parameters, especially at the top boundary with the deep ocean, and possibly also at the bottom boundary with the silicates. In their model, they monitored the melt production and assumed that the generated melt is instantaneously extracted into the overlying ocean. Thus the matrix compaction associated with the volume change due to melting did not have to be taken into account.

To understand the fate of water within the HP ice layer, a numerical model must handle a mixture composed of two phases: solid ice and liquid water. The only studies on the topic have been conducted for Ganymede by (95; 96) using a 2D Cartesian model of convection of a two-phase mixture of pure ice and water. This formalism allows a self-consistent treatment of both the melting process and

the water flow within or through the convecting solid ice (depending on the ice permeability). The two-phase simulations have confirmed some of the previous results by (35)—namely, that melting in the pure HP ice layer always occurs at the top interface with the overlying ocean in a layer of temperate ice (i.e., ice where temperature equals the melting temperature, $T$=$T_{\rm m}$). However, depending on the efficiency of convection, some melt may also be generated at the interface with the silicates as well as in the thick layer of convecting ice. Based on the thermal structure of the HP ice layer and the occurrence of melting at the interface with silicates or in the convecting ice, four different regimes of exchange between the silicates and the ocean were defined (96): (1) **direct exchange** (melting at the bottom interface as well as in the upwelling plumes), (2) **indirect exchange** (melting at the bottom interface but freezing within the convective domain), (3) **limited exchange** (only limited melting at the bottom interface), and (4) **no exchange** (no melting at the bottom interface). The temperature profiles and the corresponding exchange regimes are described in Figure 8. Note that no significant amount of water is accumulated at the silicate interface in any of the cases.

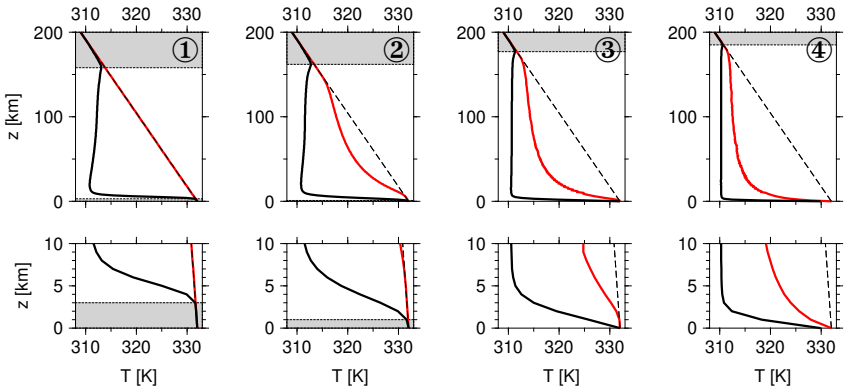


Fig. 8: Temperature profiles for each of the four exchange regimes (circled numbers). Maximum (red), horizontally-averaged (black), and melting (black dashed) temperature. Top and bottom temperate layers (gray). Bottom panels show lower10 km. Modified from (96).

The occurrence of bottom melting depends on the efficiency of thermal convection in the HP ice layer—for high Rayleigh number, the heat transfer by solid-state convection is very efficient, the temperature at the silicate interface is below the melting temperature and thus no melting occurs—this corresponds to exchange regime #4. For small Rayleigh number, the heat transfer by convection is not very efficient, the whole layer warms and melting occurs at the silicate interface. This corresponds to regimes #1 and 2, while regime #3 is a transition between these two end members. Rayleigh number increases strongly with the thickness of the HP ice layer, as $H^3$, and decreases with the ice viscosity $\mu_{\rm i}$. Thus, for a fixed viscosity, the thickening of the cooling HP ice layer with time (crystallization of the sandwiched ocean) leads to an increase of the Rayleigh number and the transition from exchange regimes with bottom melting toward the regime without bottom melting. The presence of melt at the interface between the silicate layer and the HP ice layer facilitates the transfer of volatiles from the rock into the ocean. The

exchange between the silicates and the ocean due to melting and water transport through the HP ice layer is thus more likely early in the moon's evolution when its HP ice layer is thin enough for bottom melting to occur (96). As discussed in Section 1.1, the thickness of Titan's ice crust is between 50 and 100 km and thus does not provide a strong constraint on the thickness of the HP ice layer, which can be anywhere between 50 and 300 km. For the more differentiated Ganymede, which has a much thicker hydrosphere, the presence of large impact craters suggests a thick icy crust and thus a thick HP ice layer around 400 km (e.g. 182). Consequently, melting at the HP ice/silicates interface is predicted to have occurred longer in Titan's interior, and it may be ongoing while it is less likely for Ganymede.

Based on the results of the numerical simulations, scaling laws were derived for Ganymede (96). First, the occurrence of melt at the silicates interface was investigated and scaling for a critical Rayleigh number as a function of silicate heat flux $q_s$ was found. If the Rayleigh number is larger than the critical value, melting does not occur at the silicate interface. This scaling parameterization thus predicts whether melt will occur at the silicate interface without the neeeding to perform two-phase convection simulations, and can be used in future thermal evolution models. Scaling laws were also derived for the amount of melt produced at the silicate interface and the outflowing water velocity at the ocean interface. For both, the controlling parameter is the heat flux that comes from the silicate interior (96).

One pending question is the effect of a cold ocean whose crystallization temperature is shifted toward lower temperature due to the presence of solutes. The presence of salts may result in the formation of a cold thermal boundary layer at the interface between the ocean and the HP ice layer, which can limit the transfer to the ocean. In addition, the exchange processes may be affected by the presence of salts in the melt produced at the interface between the silicates and the HP ice layer. Further work on this topic is needed in order to understand how the HP ice layer mediates the exchange between the silicate interior and the ocean.

## 4 Origin, differentiation and evolution

The present-day structures and compositions of Ganymede, Callisto, and Titan resulted from accretion and differentiation processes that likely occurred very early during the evolution of the solar system. The differences in structure and composition we can determine at present between these three moons may have been caused by subtle differences during the accretion and differentiation processes, which led to divergent evolutionary paths. In the present section, we review the state of the art concerning the origin and differentiation of large icy moons, and the implications for their evolution.

### 4.1 Accretion, impact-induced melting, and ocean formation

Most of the icy moons of Jupiter and Saturn formed in a disk that was the outgrowth of the formation of planet itself. The conditions under which the giant planet formed therefore had a direct impact on the formation of their moons (e.g.

51; 154). The evolution of the circumplanetary disk is controlled by the accretion rate of the gas and dust from the surrounding solar nebula and the growth rate of the giant planet. Many models have been proposed to describe the evolution of the disk and growth of icy satellites from it (e.g. 30; 132; 133; 51; 154). The evolution of this disk determined the composition and architecture of the whole giant planet system as well as the final assemblage that led to the formation of regular icy moons. For instance, it has been proposed that the fact that Saturn has only one big moon (Titan) while Jupiter has four could be explained by difference in gas-dust infall from the solar nebula onto the subdisk (154). According to this model, Jupiter's formation and its subsequent migration into the disk may have resulted in a slower gas infall onto Saturn and subsequently to less available mass to accrete large icy moons.

A critical aspect concerns the way solids were incorporated into the disk. Different processes have been advocated (see for instance (51) and (31) for more detailed discussions): (1) direct transport of small particles into the disk with the inflowing gas, (2) ablation and gas drag capture of planetesimals orbiting the Sun through the gas-rich circumplanetary disk, (3) break-up, dissolution and recondensation of planetesimals in the extended envelope of the forming planet, (4) collisional capture of planetesimals. These mechanisms result in differences in impactor size and velocity distribution that have major consequences for the satellite accretion (129).

The size and velocity distribution of the impactors, as well as their composition, have probably varied in space and time within the subdisk (e.g. 149), which may explain the difference in composition between the icy satellites. Two reservoirs of primitive bodies may have contributed to the satellite growth: bodies in orbit around the planet, formed or captured within the circumplanetary disk, and bodies in orbit around the Sun, colliding directly with the growing satellite (e.g. 171). The contribution of each of these two reservoirs probably varied as the circumplanetary disk evolved. When the accretion sequence started, centimeter-sized planetocentric particles were probably pre-dominant, while kilometer-sized and larger bodies became more and more frequent during the late-stage of accretion (142; 47).

By modeling the satellite accretion in 3D from a swarm of impactors of various sizes, Monteux et al.(129) tested the influence of impact size distribution on the thermal evolution of growing satellite. They showed that for satellites exceeding 1500-2000 km, surface melting can be avoided only if the satellite accreted relatively slowly ($>$ 1Myr) from small impactors ( $<$ 1 km) and if the conversion of impact energy into heat is unrealistically inefficient ($< 10--15\%$), confirming the first estimations of (14). However, as soon as a small fraction ($> 10\%$) of the impactor exceeds 1 km, global melting for large bodies like Titan or Callisto cannot be avoided. Global melting results in the formation of a surface ocean in equilibrium with a massive primitive atmosphere generating by the release of volatiles brought by the icy impactors (108; 178; 120) (see Figure 9- left column).

The post-accretional structure of a large icy moon like Titan or Ganymede thus consists of an inner undifferentiated ice-rock interior overlaid by a layer of sedimented rocks and a thick liquid water ocean, resulting from melting of the icy impactor (102; 178). A primitive atmosphere potentially exceeding 10 bars can be

maintained in equilibrium with the water ocean as long as the surface temperature exceeds the crystallization point. During this post-accretional period, the pressure at the base of the ocean is not large enough to lead to the formation of a high-pressure layer and the water ocean directly interacts with the sedimented rock layer, potentially promoting large-scale water-rock interactions and production of $CH_4$ and other gas compounds (67).

### 4.2 Heat budget and water-ice-rock segregation

During the early stages of the satellite's history three main sources of energy may have contributed to the internal thermal budget, in addition to impact heating: radiogenic heating, tidal heating associated with despinning, and viscous heating due to ice-rock separation. Differences in accretion rate and heat sources may explain the different differentiation states of Ganymede, Callisto, and Titan. Differences in the efficiency of heat and mass transfer from mixed ice-rock layers, owing to differences in post-accretional structure, may further accentuate the differentiation dichotomies. In this section, we review the various processes that may explain the divergence of ice-rock segregation and internal melting between the three large icy ocean moons (Figure 9).

Impact heating results from the deposition of impactor kinetic energy during satellite accretion and subsequent periods of intense bombardment. It therefore depends on the momentum of the impactor and the way kinetic energy is converted into heat. The impact creates a shock wave that compresses the satellite beneath the impact site. Because shock compression is an irreversible process, the entropy below the impact site increases, leading to a temperature increase. Barr et al.(13) proposed that differences in impact energy received by Ganymede and Callisto during the late heavy bombardment may explain the dichotomy between the two moons. Ganymede is closer to Jupiter than Callisto, so it is expected to experience twice as many impacts as Callisto. The impact velocity at Ganymede would have been also larger than at Callisto ($\sim 20$ km s$^{-1}$ vs $\sim 15$ km s$^{-1}$). This difference may have created large-scale melting of the outer envelop, leading to runaway differentiation in the case of Ganymede, while impact-induced melting would have been more moderate at Callisto (14).

The heat sources may also differ substantially between the three large moons, due to difference in composition and orbital configuration. Internal heating due to short-lived radioactive isotopes (mainly $^{26}$Al) probably does not play a role on these large moons. As the half-time of these short-lived elements is of the order of 1 million years, they are probably already negligible at the end of accretion of these big moons. The main heat source is provided by the decay of long-lived radiogenic elements, mostly $^{40}$K, $^{235}$U during the first billion of years. Chondrites can be used to provide some estimate of the heat power generated by the radiogenic decay of the rocky phase in the moons. For Titan, carbonaceous chondrites, which are believed to be the dominant types of chondrites beyond Jupiter (107), are commonly assumed as good proxy of the rocky phase (59; 175; 67; 136). For Jupiter's moons, LL-type ordinary chondrites have also been proposed as possible rocky phase candidates (109; 110). Depending on the assumed chondritic

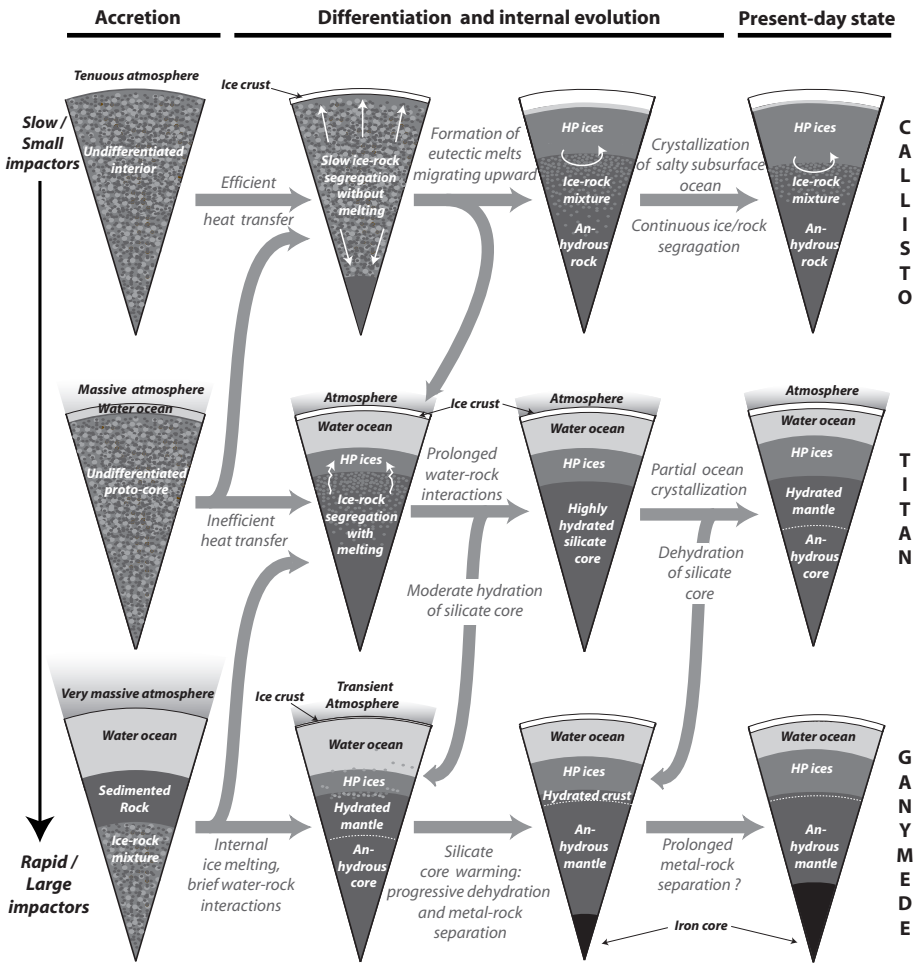


Fig. 9: Possible evolution scenarios for the interior of Callisto, Titan, and Ganymede assuming different initial states. Depending mostly on the efficiency of heat transfer in the interior, different bifurcations in the evolutionary path may have occurred explaining the present-day state of their interior. The interior structure shown here are just possible interior structures compatible with existing observational constraints. Existing data are, however, not sufficient to conclude with certitude concerning the differentiation state of these moons (Adapted from Tobie et al. (178))
.

composition, the initial radiogenic power may vary between 2.8 and 4.6 TW for Ganymede, and 1.9 and 3.2 TW for Callisto (85). For Titan, if we assume a composition dominated by CI chondrites, the total power should not exceed 2.5 TW (85).

Differences in tidal heating might also explain the dichotomies between these moons. Due to its closer distance to Jupiter and its interaction with Io and Europa

through the Laplace resonance, Ganymede likely experienced more tidal heating than Callisto during its evolution (161; 19). In particular, Malhotra (118) and Showman et al.(161) suggested that the Galilean satellites passed through one or more Laplace-like resonances before evolving into the current Laplace resonance, resulting in prolonged periods with enhanced eccentricity and tidal dissipation in Ganymede (19; 20). By contrast, Callisto's eccentricity probably remained small (0.007 at present) during its evolution, resulting in very small tidal forcing due to the distance to Jupiter (85). Tidal forces on Titan raised by Saturn are comparable to those experienced by Callisto. However, as Titan's eccentricity is larger (0.0294 at present), this leads to large time variations of tidal forces, resulting in more tidal energy potentially dissipated. The elevated eccentricity of Titan in the absence of orbital resonances suggests that the present-day value is the remnant from Titan's early evolution when it may have experienced tidal heating comparable to Europa's (176; 177). Simultaneously with their accretion, the moons also experienced strong tidal despinning to tidally-locked spin-orbit resonances. Although the associated dissipation rate is large, it lasted for short periods of time, on the order of 100,000 years (85), resulting in a moderate increase of internal temperature of 25-50 K (178).

A final source of energy resulted from the release of gravitational energy associated to internal differentiation (63; 85; 178). The increase of temperature associated with the change of gravitational energy between an initially homogeneous interior and a differentiated interior with a full separation of rock and ice phases is of the order of 100-150 K. If the ice-rock separation is fast enough ($< 0.5$ Gyr), the dissipation of potential energy may induce runaway melting and thus may create a catastrophic differentiation, as has been proposed for Ganymede (63; 102). This early period corresponds to the first stage of evolution for Ganymede in Figure 9. If the differentiation process is slow and more gradual ($> 1$ Gyr), the convective heat transfer should be able to transport the additional energy, preventing internal melting, as proposed for Callisto (134) (see Figure 9 - first row). O'Rourke and Stevenson (144) showed, using Titan as an example, that double-diffusive convection in a mixed ice-rock interior can delay internal melting and ice-rock separation, but cannot prevent it, even if reduced radiogenic power is assumed (see Figure 9—second row). This indicates that it may be difficult to prevent full ice-rock separation. If Callisto is not fully differentiated, then it would be a mystery in this regard. We should keep in mind, however, that ice-rock separation depends on the rheology of ice-rock mixtures, which is poorly constrained at high pressures. Further experimental and modeling efforts are required to better understand the differentiation processes of large icy moons.

Throughout the differentiation process, internal melting may contribute to the efficiency of heat transfer, which has not been quantified so far. Melt migration is an efficient way to transport heat and to favor chemical exchange. The compositions of internal oceans have almost certainly been conditioned by leaching processes (Figure 9). Though some studies have focused on this topic, especially for Titan (50; 32; 59), work is needed to understand the interplay between ice-rock segregation, fluid generation and transport, and leaching in large ocean worlds.

### 4.3 Iron core formation and core-mantle-hydrosphere evolution

The presence of an iron core depends on the degree of differentiation. As mentioned previously, Callisto and Titan seem to be only moderately differentiated—the rock+metal and ice phases may have been separated only incompletely (e.g., 8; 87). Furthermore, both satellites lack an intrinsic magnetic fields (100; 12), which is consistent with their partial differentiation. In contrast, Ganymede's low moment of inertia (MoI) (e.g. 9) and intrinsic magnetic field (104) suggest a fully differentiated interior—further differentiation of the rock+metal primordial core into a metallic core and an overlying rocky mantle (Figure 9 - third row). Characterized by five flybys of the *Galileo* spacecraft, the magnetic field is predominantly dipolar, with an equatorial surface field strength of 719 nT and a tilt away from the spin axis of $4^o$ (104). Ganymede's unique magnetic field is most likely driven by a core dynamo, where the kinetic energy is converted to magnetic energy. Core flows are likely driven by convection (e.g. 75); libration-driven elliptical instability is likely absent (114) although precession-driven flows may be possible. The existence of Ganymede's magnetic field implies that the central iron alloy core is at least partially liquid. Estimates of the core's size range from one-quarter to one-third of the satellite's radius (165). Core composition is similarly open question, with sulfur often assumed as the dominant light element (e.g. 157; 155), although other elements such as oxygen are also likely present (146).

McKinnon (123) and Spohn et al. (170) showed that, once ice and rock-metal phases are fully separated, radiogenic heating in the rock+metal phase is sufficient to raise the temperature to the Fe-FeS melting temperature. Such heating, however, may take several hundred million years assuming insignificant heat escape during this time (170). If enough melt is generated, it may permeate downwards to form a metal-rich core (e.g. 195). The slightly lower rock fraction of Callisto and Titan and therefore lower radiogenic heating compared to Ganymede could be another reason for only partial differentiation of these two (155).

In the present day, tidal heating probably contributes insignificant heat to Ganymede, Callisto, and Titan. While tidal heating probably never played an important role in Callisto's history, it might have for Ganymede and Titan (e.g. 161; 164; 19; 179). Transfer of heat in icy satellites is dominated by heat conduction and convection. As also discussed in Section 3.2, thermal convection occurs if the Rayleigh number—the ratio of diffusive and advective heat transport—exceeds a critical value. While convection is likely to occur in the putative liquid reservoirs of icy satellites like an ocean or a metallic core, it can be harder to achieve in the solid parts like the rocky mantle or the ice I crust (or high-pressure ice phases). The onset of convection depends on the viscosity, the thermal properties, and the size of the satellite. Different scenarios illustrating the basic mechanisms have been calculated by Ellsworth et al.(48) for the small Saturnian satellites. If convection occurs in the rocky mantle, it likely operates in the stagnant lid mode due the strongly temperature-dependent viscosity of silicates and water ice (e.g. 156). Convection then takes place below a rigid shell, across which heat is transported less efficiently via conduction.

If a metal core exists, which is the case for Ganymede, cooling of that core presents another heat source to the overlying rocky mantle and hydrosphere. Even though heat transport within the core is efficient due to convection, cooling of the core is limited to the amount of heat that can be extracted by the much more slowly convecting rocky mantle. The rocky mantle and metallic core are coupled via the temperature at the core-mantle boundary (CMB). If the core temperature has cooled sufficiently to drop below the melting point of the core alloy, the core will start to freeze. The latent heat released during freezing slows cooling at the CMB, temporarily delaying cooling of the mantle (e.g., 173).

Based on experimental work with low-pressure Fe-FeS alloys, core differentiation in small planetary bodies like Ganymede may substantially differ from Earth's inner core growth (54; 53; 55; 41; 130; 131; 28). Instead of freezing from the inside out, the core solidifies from the top to the bottom (123; 75; 194). Thermal evolution models of metallic cores are important for estimating the power available to a potential dynamo.

Thermal evolution models have focused mostly on understanding how a satellite with a small iron core could have an active magnetic field at present day. Although thermal convection has been considered (101), most studies have relied on thermo-compositional convection (75; 19; 151; 153). In this mode, compositional buoyancy is associated with the sinking of Fe snow, assuming top-down core solidification for an iron-rich composition or with the upward flotation of solid FeS if the core is more sulfur-rich than the eutectic (24). Rückriemen et al.(153), for example, argued that both of these regimes can explain Ganymede's magnetic field, although dynamos driven by iron snow are generally young (less than 1 Ga) while FeS flotation dynamos can be up to 3.8 Ga.

Dynamo models simulating convection and magnetic field generation in the core are complementary to these studies. Zhan and Schubert (196) showed that dynamo properties differ depending on the core crystallization regime and conclude that FeS flotation is most consistent with a dipole-dominated magnetic field, while Christensen et al. (40) showed that convection driven by iron snow can reproduce Ganymede's observed dipole moment as well as its anomalously low quadrupole component. The contrasting conclusions of these studies is primarily a consequence of the different assumed source regions for compositional buoyancy (i.e., volumetric versus boundary origins) and the absence/presence of an outer stably-stratified layer in the model.

## 5 Discussion and perspectives

### 5.1 Habitability

In the last ten years, progress in understanding the formation and evolution of large icy moons has come from the observations of Titan by the *Cassini-Huygens* mission, progress on numerical modeling, and a wealth of new laboratory data. However, the question of the degree of habitability of these large icy moons is far

from being solved.

The global fluxes of chemical energy must be understood in terms of a world's interior structure and evolution (186). Such a global picture is necessary for quantifying the types of life and amounts of biomass that might be supported (160). A global perspective is also required for interpreting any potential indications of life that might be found through in-situ sampling, as, for example, by a lander on Europa's surface (74). In light of recent progress on the occurrence and potential stability of fluids within and underneath high-pressure ices (35; 95), it no longer seems to be the case that the presence of such ices impedes water-rock interactions altogether. A greater concern for the availability of chemical energy where high-pressure ices occur may be that the surface areas available for water-rock exchange are limited. High pressures at the water-rock interface ($>$ 250 MPa) may force the elastic closure of fractures (185) and prevent tectonic opening (29). These considerations are also directly relevant to the habitability of ocean worlds that may be present around other stars (117) for which the three large solar icy moons can be used as proxi.

## 5.2 Ocean exoplanets

The number of detected exoplanets has grown exponentially thanks to the Kepler data. Among those planets, some may have a thick hydrosphere overlying a rocky interior (97; 139; 140). In applying the ideas discussed here to larger exo-ocean worlds, it is important to distinguish between water-rich super-Earths and mini-Neptunes. It appears that a population gap around 1.8 Earth radii ($R_{Earth}$) separates these two populations, with the larger planets potentially richer in volatile species (64; 112). Like the solar system's ice giants Uranus and Neptune, mini-Neptunes would contain layers of super-ionic fluid and ices at extreme pressures and temperatures, potentially mixing with their rocky core (diffuse structure rather than layered), incompatible with the type of habitability discussed in this chapter. Therefore, exo-ocean worlds refers here to water-rich super-Earths with radii below $1.8R_{Earth}$.

These exoplanets, also referred to as ocean planets (117), are much larger than Ganymede, and their interior structure, inferred from first principles, predicts that their hydrosphere would be dominated by high pressure ices (VII and X)(167; 139). Recent data on the characteristics of ice VII and X (17; 106; 91; 77) can be used in further modeling to understand the possible hydrosphere structures and evolution of such planets. Nonetheless, many aspects remain largely unconstrained by experiment or theory, such as the rheology of these ultra high-pressure ices, as well as the possible water/ice-rock interactions at gigapascal pressures and $>$1000K temperatures, important for understanding thermal and chemical transport and potential for habitability of their ocean (139).

Depending on their orbital distances and the chemistry of their atmospheres (e.g., a hydrogen-helium dominated atmosphere or a carbon-dioxide rich atmosphere), the surface temperatures of exo-ocean worlds can also be high enough to allow for liquid water at the surface, such that the ocean may be in direct contact with the atmosphere. (103) showed that the existence of a high-pressure layer

would lead to a different carbon cycle than on a rocky planet covered by water, since the carbonate-silicate cycle would not be active on such planets. Instead, the climate would be determined by the solubility of carbon dioxide in the oceans, and could potentially be very unstable. Future studies are needed to understand the equilibria between atmosphere and ocean on such planets, to predict if, for example, reducing atmospheres similarly to Titan's would be possible, or if carbon- or nitrogen-dominated atmospheres are likely to exist for ocean planets.

### 5.3 Geochemical exchange processes

The ability of the HP ice layer to transfer compounds from the rocky core to the ocean is key to understanding the conductivity of the ocean. It is also important to determine whether salty layers can form and exist stably between the different types of HP ice, and also between the HP ice and the silicate layer (92; 183; 139). In the case of pure water, it was demonstrated (95) that only a few percent of melt can be present at the interface with the silicates. Contrary to the terrestrial equivalent of subglacial lakes where water is denser than ice I, HP ice is denser than water. As a result, the presence of water adds to the buoyancy of the ice and favors its upwelling. To make water denser requires the addition of salt in amounts on the order of 10 wt% (92; 184). Numerical simulations that can handle the complexities of salts which create eutectics and can concentrate in pockets will have to be addressed in the future.

The terrestrial ocean is characterized by the presence of hydrothermal vents where autotrophic communities of organisms reside indepedent from the sun's energy. Such vents have been proposed as places where life may have emerged. They are settings with gradients in pH and redox between the ocean and the fluids circulating in the oceanic crust (152). Such hydrothermal activity has been inferred to occur in Enceladus based on the analysis of ice grains ejected from Enceladus's interior (83; 159; 147). However, the presence of gradients between the water circulating in the rocks and the ocean is not established. Recent models for Enceladus (34) suggest that the ocean circulates into the porous rocky core, indicative of chemical equilibrium. Enceladus pressure is low and porosity can be large. On the large icy moons, the percolation of fluids may be more limited. One process may be the cracking of the crust due to serpentinization of the rock (99). It is still unknown whether such processes could exist in the upper part of the rocky core of large icy moons. Numerical modelling of such environments may help in understanding the interaction between a hydrated core and a HP ice layer. Finally, it is worth recalling that Titan may not have had a HP ice layer during much of its history, and that conditions at the ocean-silicate interface may have resembled those at Europa, albeit with higher pressures at the water-rock interaface.

### 5.4 Space missions and experimental perspectives

A better understanding of the role of high-pressure ices on the habitability of large icy moons will require progress in numerical simulations, more laboratory experiments to measure the parameters in the (P,T) range of interest, and observations from space missions. Two missions are in development: the ESA-led

JUICE mission to Callisto and Ganymede (68), and the NASA Dragonfly mission to Titan (180). The JUICE mission is equipped with a radar sounder and magnetometer whose data should provide precise thickness of Ganymede's ice crust, which strongly constrains the depth of the ocean-HP ice interface (182). In addition, the interpretation of the magnetic data (conductivity of the ocean) and the gravity data (density of the ocean through the moment of inertia and value of the tidal Love number $k_2$) should provide constraints on the thickness and salinity of the ocean. These data will be key to inferring the thickness of the HP ice layer and assessing its dynamics and the transfer of volatiles from the silicates to the ocean. The Dragonfly mission will land at different places on Titan's surface. It is equipped with a geophysical package including seismometers that could determine the thickness of the ice crust and characterize its dynamics. It may also provide information about the deep interior if the seismic activity triggered by tidal forces along Titan's highly eccentric orbit around Saturn is high enough and allows the sensors to record seismic waves propagating deep into Titan's interior (172).

As demonstrated in the Section 2, the effect of high pressures in large ocean-worlds cannot be correctly extrapolated from data collected in well-studied ranges below 100 MPa. If equilibrium properties can be derived from thermodynamic potentials based on a few parameters (e.g., sound speed, density), transport properties (especially the rheology) need to be measured independently at the relevant conditions. Few studies have characterizied and quantifyied the creep behavior of high-pressure ice polymorphs at the small strain rates occurring in icy ocean worlds. In addition, there is no ice VII creep law to date, although it may be a major constituent of the hydrospheres of exo-oceans.

Furthermore, there is evidence that new major phases remain to be discovered and characterized at high pressure, as compression allows stabilization of new crystallographic configurations in non-pure system, as suggested for the $H_2O$-NaCl binary (181). Even in modest amounts, these phases could considerably influence the bulk physical properties of the ice dominated layers (upper ice crust and high pressure ices mantle) and the chemical transport through the hydrosphere, but remain largely unconstrained to date.

These are a few examples of laboratory experiments that should be carried out as they are critical to the interpretation of data acquired by space missions. The development of the JUICE and Dragonfly missions should be a lever for the funding of such laboratory experiments.

**Acknowledgements** B.J. was supported by the NASA Postdoctoral Program fellowship, other University of Washington authors were supported by the NASA Solar System Workings Grant 80NSSC17K0775 and by the Icy Worlds node of NASA's Astrobiology Institute (08-NAI5-0021).

K.K. was supported by the Czech Science Foundation through project No. 19-10809S and by Charles University Research program No. UNCE/SCI/023.

Work by JPL co-authors was partially supported by strategic research and technology funds from the Jet Propulsion Laboratory, Caltech, and by the Icy Worlds and Titan nodes of NASA's Astrobiology Institute (13-13NAI7_2-0024 and 17-NAI8-2-017).

K.M.S. was supported by NASA Grant NNX14AR28G.

## References


1. Abramson, E.H., Bollengier, O., Brown, J.M.: Water-carbon dioxide solid phase equilibria at pressures above 4 GPa. Scientific Reports **7**(1), 821 (2017). DOI 10.1038/s41598-017-00915-0
2. Abramson, E.H., Bollengier, O., Michael, B.J., Journaux, B., Kaminsky, W., Pakhomova, A.: Carbonic acid monohydrate. American Mineralogist **103**(9), 1468–1472 (2018). DOI 10.2138/am-2018-6554
3. Adams, L.: Equilibrium in binary systems under pressure. I. An experimental and thermodynamic investigation of the system, NaCl-H2o, at 25. Journal of the American Chemical Society **53**, 3769–3813 (1931)
4. Adams, L.H., Hall, R.E.: The Effect of Pressure on the Electrical Conductivity of Solutions of Sodium Chloride and of Other Electrolytes. The Journal of Physical Chemistry **35**(8), 2145–2163 (1930). DOI 10.1021/j150326a001
5. Aleksandrov, A.A., Dzhuraeva, E.V., Utenkov, V.F.: Thermal conductivity of sodium chloride aqueous solutions. Thermal Engineering **60**(3), 190–194 (2013). DOI 10.1134/S0040601513030026
6. Amos, D.M., Donnelly, M.E., Teeratchanan, P., Bull, C.L., Falenty, A., Kuhs, W.F., Hermann, A., Loveday, J.S.: A Chiral Gas–Hydrate Structure Common to the Carbon Dioxide–Water and Hydrogen–Water Systems. The Journal of Physical Chemistry Letters **8**(17), 4295–4299 (2017). DOI 10.1021/acs.jpclett.7b01787
7. Anderson, J.: Shape, mean radius, gravity field, and interior structure of Callisto. Icarus **153**(1), 157–161 (2001). DOI 10.1006/icar.2001.6664
8. Anderson, J., Schubert, G., Jacobson, R., Lau, E., Moore, W., Sjogren, W.: Distribution of rock, metals, and ices in Callisto. Science **280**(5369), 1573 – 1576 (1998)
9. Anderson, J.D., Lau, E.L., Sjogren, W.L., Schubert, G., Moore, W.B.: Gravitational constraints on the internal structure of Ganymede. Nature **384**(6609), 541–543 (1996). DOI 10.1038/384541a0
10. Andersson, O., Inaba, A.: Thermal conductivity of crystalline and amorphous ices and its implications on amorphization and glassy water. Physical chemistry chemical physics: PCCP **7**(7), 1441–1449 (2005)
11. Atreya, S.K., Donahue, T.M., Kuhn, W.R.: Evolution of a nitrogen atmosphere on Titan. Science **201**(4356), 611–613 (1978)
12. Backes, H., Neubauer, F.M., Dougherty, M.K., Achilleos, N., André, N., Arridge, C.S., Bertucci, C., Jones, G.H., Khurana, K.K., Russell, C.T., et al.: Titan's magnetic field signature during the first cassini encounter. Science **308**(5724), 992–995 (2005)
13. Barr, A.C., Canup, R.M.: Origin of the Ganymede-Callisto dichotomy by impacts during the late heavy bombardment. Nature Geoscience **3**, 164–167 (2010). DOI 10.1038/ngeo746
14. Barr, A.C., Citron, R.I., Canup, R.M.: Origin of a partially differentiated Titan. Icarus **209**, 858–862 (2010). DOI 10.1016/j.icarus.2010.05.028
15. Béghin, C., Randriamboarison, O., Hamelin, M., Karkoschka, E., Sotin, C., Whitten, R.C., Berthelier, J.J., Grard, R., Simões, F.: Analytic theory of Titan's Schumann resonance: Constraints on ionospheric conductivity and buried water ocean. Icarus **218**(2), 1028–1042 (2012)

16. Bercovici, D., Schubert, G., Reynolds, R.T.: Phase transitions and convection in icy satellites. Geophysical Research Letters **13**(5), 448–451 (1986). DOI 10.1029/GL013i005p00448
17. Bezacier, L., Journaux, B., Perrillat, J.P., Cardon, H., Hanfland, M., Daniel, I.: Equations of state of ice VI and ice VII at high pressure and high temperature. Journal of Chemical Physics **141**(10), 104505 (2014). DOI 10.1063/1.4894421
18. Bezacier, L., Le Menn, E., Grasset, O., Bollengier, O., Oancea, A., Mezouar, M., Tobie, G.: Experimental investigation of methane hydrates dissociation up to 5 GPa: Implications for Titan's interior. Physics of the Earth and Planetary Interiors **229**, 144–152 (2014). DOI 10.1016/j.pepi.2014.02.001
19. Bland, M.T., Showman, A.P., Tobie, G.: The production of Ganymede's magnetic field. Icarus **198**, 384–399 (2008). DOI 10.1016/j.icarus.2008.07.011
20. Bland, M.T., Showman, A.P., Tobie, G.: The orbital–thermal evolution and global expansion of Ganymede. Icarus **200**(1), 207–221 (2009). DOI 10.1016/j.icarus.2008.11.016
21. Bollengier, O., Brown, J.M., Shaw, G.H.: Thermodynamics of pure liquid water: Sound speed measurements to 700 mpa down to the freezing point, and an equation of state to 2300 mpa from 240 to 500 k. The Journal of Chemical Physics **151**(5), 054501 (2019)
22. Bollengier, O., Choukroun, M., Grasset, O., Le Menn, E., Bellino, G., Morizet, Y., Bezacier, L., Oancea, A., Taffin, C., Tobie, G.: Phase equilibria in the H2o–CO2 system between 250–330 K and 0–1.7 GPa: Stability of the CO2 hydrates and H2o-ice VI at CO2 saturation. Geochimica et Cosmochimica Acta **119**, 322–339 (2013). DOI 10.1016/j.gca.2013.06.006
23. Bove Livia E., Ranieri Umbertoluca: Salt- and gas-filled ices under planetary conditions. Philosophical Transactions of the Royal Society A: Mathematical, Physical and Engineering Sciences **377**(2146), 20180262 (2019). DOI 10.1098/rsta.2018.0262
24. Breuer, D., Rückriemen, T., Spohn, T.: Iron snow, crystal floats, and inner-core growth: modes of core solidification and implications for dynamos in terrestrial planets and moons. Progress in Earth and Planetary Science **2**(1), 1 (2015)
25. Bridgman, P.W.: Water, in the liquid and five solid forms, under pressure. Proceedings of the American Academy of Arts and Sciences **47**(13), 441–558 (1912)
26. Bridgman, P.W.: The Phase Diagram of Water to 45,000 kg/cm2. The Journal of chemical physics **5**(12), 964–966 (1937). DOI 10.1063/1.1749971
27. Brown, J.M.: Local basis function representations of thermodynamic surfaces: Water at high pressure and temperature as an example. Fluid Phase Equilibria **463**, 18–31 (2018). DOI 10.1016/j.fluid.2018.02.001
28. Buono, A., Walker, D.: The fe-rich liquidus in the fe-fes system from 1bar to 10gpa. Geochimica et Cosmochimica Acta **75**(8), 2072–2087 (2011)
29. Byrne, P.K., Regensburger, P.V., Klimczak, C., Bohnenstiehl, D.R., Hauck II, S.A., Dombard, A.J., Hemingway, D.J.: The geology of the rocky bodies inside Enceladus, Europa, Titan, and Ganymede. In: 49th Lunar and Planetary Science Conference, p. Abstract #2905. Lunar and Planetary Institute, Houston (2018)

30. Canup, R.M., Ward, W.R.: Formation of the Galilean Satellites: Conditions of Accretion. Astron. J. **124**, 3404–3423 (2002). DOI 10.1086/344684
31. Canup, R.M., Ward, W.R.: Origin of Europa and the Galilean Satellites, p. 59 (2009)
32. Castillo-Rogez, J.C., Lunine, J.I.: Evolution of Titan's rocky core constrained by Cassini observations. Geophysical Research Letters **37**(20) (2010)
33. Cavazzoni, C.: Superionic and Metallic States of Water and Ammonia at Giant Planet Conditions. Science **283**(5398), 44–46 (1999). DOI 10.1126/science.283.5398.44
34. Choblet, G., Tobie, G., Sotin, C., Běhounková, M., Čadek, O., Postberg, F., Souček, O.: Powering prolonged hydrothermal activity inside Enceladus. Nature Astronomy **1**(12), 841–847 (2017). DOI 10.1038/s41550-017-0289-8
35. Choblet, G., Tobie, G., Sotin, C., Kalousová, K., Grasset, O.: Heat transport in the high-pressure ice mantle of large icy moons. Icarus **285**, 252–262 (2017). DOI 10.1016/j.icarus.2016.12.002
36. Chou, I.M., Seal, R.R.: Magnesium and calcium sulfate stabilities and the water budget of Mars. Journal of Geophysical Research: Planets **112**(E11) (2007). DOI 10.1029/2007JE002898
37. Choukroun, M., Grasset, O.: Thermodynamic model for water and high-pressure ices up to 2.2 GPa and down to the metastable domain. The Journal of chemical physics **127**(12), 124506 (2007)
38. Choukroun, M., Grasset, O.: Thermodynamic data and modeling of the water and ammonia-water phase diagrams up to 2.2 GPa for planetary geophysics. The Journal of Chemical Physics **133**(14), 144502–144502–13 (2010). DOI 10.1063/1.3487520
39. Choukroun, M., Kieffer, S.W., Lu, X., Tobie, G.: Clathrate Hydrates: Implications for Exchange Processes in the Outer Solar System. In: The Science of Solar System Ices, Astrophysics and Space Science Library, pp. 409–454. Springer, New York, NY (2013). DOI 10.1007/978-1-4614-3076-6$_1$2
40. Christensen, U.: Iron snow dynamo models for ganymede. Icarus **247**, 248–259 (2015)
41. Chudinovskikh, L., Boehler, R.: Eutectic melting in the system fe-s to 44 gpa. Earth and Planetary Science Letters **257**(1), 97–103 (2007)
42. Dunaeva, A.N., Antsyshkin, D.V., Kuskov, O.L.: Phase diagram of H2o: Thermodynamic functions of the phase transitions of high-pressure ices. Solar System Research **44**(3), 202–222 (2010). DOI 10.1134/S0038094610030044
43. Durham, W., Kirby, S., Stern, L.: Creep of water ices at planetary conditions: A compilation. Journal of geophysical research **102**(E7), 16293–16302 (1997)
44. Durham, W., Prieto-Ballesteros, O., Goldsby, D., Kargel, J.: Rheological and thermal properties of icy materials. Space science reviews **153**(1), 273–298 (2010)
45. Durham, W., Stern, L., Kirby, S.: Rheology of water ices v and vi. Journal of geophysical research **101**(B2), 2989–3001 (1996)
46. Durham, W.B., Kirby, S.H., Stern, L.A., Zhang, W.: The strength and rheology of methane clathrate hydrate. Journal of Geophysical Research: Solid Earth **108**(B4) (2003). DOI 10.1029/2002JB001872
47. Dwyer, C., Nimmo, F., Ogihara, M., Ida, S.: The influence of imperfect accretion and radial mixing on ice: rock ratios in the galilean satellites. Icarus **225**(1), 390–402 (2013)

48. Ellsworth, K., Schubert, G.: Saturn's icy satellites: Thermal and structural models. Icarus **54**(3), 490–510 (1983)
49. Engel, E.A., Anelli, A., Ceriotti, M., Pickard, C.J., Needs, R.J.: Mapping uncharted territory in ice from zeolite networks to ice structures. Nature Communications **9**(1), 2173 (2018). DOI 10.1038/s41467-018-04618-6
50. Engel, S., Lunine, J.I., Norton, D.L.: Silicate interactions with ammonia-water fluids on early Titan. J. Geophys. Res. **99**, 3745–3752 (1994). DOI 10.1029/93JE03433
51. Estrada, P.R., Mosqueira, I., Lissauer, J.J., D'Angelo, G., Cruikshank, D.P.: Formation of Jupiter and Conditions for Accretion of the Galilean Satellites, p. 27 (2009)
52. Falenty, A., Hansen, T.C., Kuhs, W.F.: Formation and properties of ice XVI obtained by emptying a type sII clathrate hydrate. Nature **516**(7530), 231–233 (2014). DOI 10.1038/nature14014
53. Fei, Y., Bertka, C.M., Finger, L.W.: High-pressure iron-sulfur compound, $Fe_3S_2$, and melting relations in the Fe-FeS system. Science **275**(5306), 1621–1623 (1997)
54. Fei, Y., Li, J., Bertka, C., Prewitt, C.: Structure type and bulk modulus of fe3s, a new iron-sulfur compound. American Mineralogist **85**(11-12), 1830–1833 (2000)
55. Fei, Y., Prewitt, C., Mao, H., Bertka, C., et al.: Structure and density of fes at high pressure and high temperature and the internal structure of mars. Science (New York, NY) **268**(5219), 1892 (1995)
56. Feistel, R., Wagner, W.: A New Equation of State for H2o Ice Ih. Journal of Physical and Chemical Reference Data **35**(2), 1021–1047 (2006). DOI 10.1063/1.2183324
57. Fletcher, N.H.: The Chemical Physics of Ice. Cambridge University Press (1970)
58. Fortes, A., Grindrod, P., Trickett, S., Vocadlo, L.: Ammonium sulfate on Titan: Possible origin and role in cryovolcanism. Icarus **188**(1), 139–153 (2007). DOI 10.1016/j.icarus.2006.11.002
59. Fortes, A.D.: Titan's internal structure and the evolutionary consequences. Plan. Space Sci. **60**, 10–17 (2012). DOI 10.1016/j.pss.2011.04.010
60. Fortes, A.D., Choukroun, M.: Phase Behaviour of Ices and Hydrates. Space Science Reviews **153**, 185–218 (2010). DOI 10.1007/s11214-010-9633-3
61. Fortes, A.D., Wood, I.G., Alfredsson, M., Vočadlo, L., Knight, K.S., Marshall, W.G., Tucker, M.G., Fernandez-Alonso, F.: The high-pressure phase diagram of ammonia dihydrate. High Pressure Research **27**(2), 201–212 (2007). DOI 10.1080/08957950701265029
62. French, M., Redmer, R.: Construction of a thermodynamic potential for the water ices VII and X. Physical Review B **91**(1), 014308 (2015). DOI 10.1103/PhysRevB.91.014308
63. Friedson, A.J., Stevenson, D.J.: Viscosity of rock-ice mixtures and applications to the evolution of icy satellites. Icarus **56**, 1–14 (1983). DOI 10.1016/0019-1035(83)90124-0
64. Fulton, B.J., Petigura, E.A., Howard, A.W., Isaacson, H., Marcy, G.W., Cargile, P.A., Hebb, L., Weiss, L.M., Johnson, J.A., Morton, T.D., et al.: The california-kepler survey. iii. a gap in the radius distribution of small planets. The Astronomical Journal **154**(3), 109 (2017)
65. Gao, P., Stevenson, D.J.: Nonhydrostatic effects and the determination of icy satellites' moment of inertia. Icarus **226**(2), 1185–1191 (2013). DOI 10.1016/j.icarus.2013.07.034

66. Giovambattista, N., Amann-Winkel, K., Loerting, T.: Amorphous ices. Liquid Polymorphism **152**, 139–173 (2013)
67. Glein, C.R.: Noble gases, nitrogen, and methane from the deep interior to the atmosphere of Titan. Icarus **250**, 570–586 (2015). DOI 10.1016/j.icarus.2015.01.001
68. Grasset, O., Dougherty, M., Coustenis, A., Bunce, E., Erd, C., Titov, D., Blanc, M., Coates, A., Drossart, P., Fletcher, L., Hussmann, H., Jaumann, R., Krupp, N., Lebreton, J.P., Prieto-Ballesteros, O., Tortora, P., Tosi, F., Hoolst, T.V.: JUpiter ICy moons Explorer (JUICE): An {ESA} mission to orbit Ganymede and to characterise the Jupiter system. Planetary and Space Science **78**(0), 1 – 21 (2013). DOI 10.1016/j.pss.2012.12.002
69. Grasset, O., Sotin, C.: The cooling rate of a liquid shell in Titan's interior. Icarus **123**(1), 101–112 (1996)
70. Grindrod, P., Fortes, A., Nimmo, F., Feltham, D., Brodholt, J., Vocadlo, L.: The long-term stability of a possible aqueous ammonium sulfate ocean inside titan. Icarus **197**(1), 137–151 (2008). DOI 10.1016/j.icarus.2008.04.006
71. Grindrod, P., Fortes, A., Nimmo, F., Feltham, D., Brodholt, J., Vočadlo, L.: The long-term stability of a possible aqueous ammonium sulfate ocean inside Titan. Icarus **197**(1), 137–151 (2008)
72. Gromnitskaya, E.L., Yagafarov, O.F., Lyapin, A.G., Brazhkin, V.V., Wood, I.G., Tucker, M.G., Fortes, A.D.: The high-pressure phase diagram of synthetic epsomite (MgSO4·7h2o and MgSO4·7d2o) from ultrasonic and neutron powder diffraction measurements. Physics and Chemistry of Minerals **40**(3), 271–285 (2013). DOI 10.1007/s00269-013-0567-7
73. Hammond, N.P., Barr, A.C.: Formation of Ganymede's grooved terrain by convection-driven resurfacing. Icarus **227**, 206–209 (2014). DOI 10.1016/j.icarus.2013.08.024
74. Hand, K.P., Murray, A.E., Garvin, J.B., Brinckerhoff, W.B., Christner, B.C., Edgett, K.S., Ehlmann, B.L., German, C., Hayes, A.G., Hoehler, T.M., Horst, S.M., Lunine, J.I., Nealson, K.H., Paranicas, C., Schmidt, B.E., Smith, D.E., Rhoden, A.R., Russell, M.J., Templeton, A.S., Willis, P.A., Yingst, R.A., Phillips, C.B., Cable, M.L., Craft, K.L., Hofmann, A.E., Nordheim, T.A., Pappalardo, R.P., the Project Engineering Team: Report of the Europa Lander Science Definition Team. Tech. rep., Jet Propulsion Laboratory, California Institute of Technology (2017)
75. Hauck II, S.A., Aurnou, J.M., Dombard, A.J.: Sulfur's impact on core evolution and magnetic field generation on Ganymede. Journal of geophysical research **111**(E9), E09008 (2006)
76. Hemingway, D., Nimmo, F., Zebker, H., Iess, L.: A rigid and weathered ice shell on Titan. Nature **500**(7464), 550–552 (2013). DOI 10.1038/nature12400
77. Hernandez, J.A., Caracas, R.: Proton dynamics and the phase diagram of dense water ice. The Journal of Chemical Physics **148**(21), 214501 (2018). DOI 10.1063/1.5028389
78. Hirai, H., Komatsu, K., Honda, M., Kawamura, T., Yamamoto, Y., Yagi, T.: Phase changes of CO2 hydrate under high pressure and low temperature. The Journal of Chemical Physics **133**(12), 124511 (2010). DOI 10.1063/1.3493452
79. Ho, P.C., Palmer, D.A., Mesmer, R.E.: Electrical conductivity measurements of aqueous sodium chloride solutions to 600C and 300 MPa. Journal of Solution Chemistry **23**(9), 997–1018 (1994). DOI 10.1007/BF00974100
80. Hogenboom, D.: Magnesium sulfate-water to 400 MPa using a novel piezometer: Densities, phase equilibria, and planetological implications. Icarus **115**(2), 258–277

(1995). DOI 10.1006/icar.1995.1096
81. Holten, V., Sengers, J.V., Anisimov, M.A.: Equation of State for Supercooled Water at Pressures up to 400 MPa. Journal of Physical and Chemical Reference Data **43**(4), 043101 (2014). DOI 10.1063/1.4895593
82. Horne, R.A., Frysinger, G.R.: The effect of pressure on the electrical conductivity of sea water. Journal of Geophysical Research **68**(7), 1967–1973 (1963). DOI 10.1029/JZ068i007p01967
83. Hsu, H.W., Postberg, F., Sekine, Y., Shibuya, T., Kempf, S.D., Horányi, M., Juhász, A., Altobelli, N., Suzuki, K., Masaki, Y., et al.: Ongoing hydrothermal activities within Enceladus. Nature **519**(7542), 207 (2015)
84. Hudleston, P.J.: Structures and fabrics in glacial ice: A review. Journal of Structural Geology **81**, 1–27 (2015). DOI 10.1016/j.jsg.2015.09.003
85. Hussmann, H., Choblet, G., Lainey, V., Matson, D.L., Sotin, C., Tobie, G., van Hoolst, T.: Implications of Rotation, Orbital States, Energy Sources, and Heat Transport for Internal Processes in Icy Satellites. Space Sci. Res. **153**, 317–348 (2010). DOI 10.1007/s11214-010-9636-0
86. Iess, L., Jacobson, R.A., Ducci, M., Stevenson, D.J., Lunine, J.I., Armstrong, J.W., Asmar, S.W., Racioppa, P., Rappaport, N.J., Tortora, P.: The tides of Titan. Science **337**(6093), 457–459 (2012). DOI 10.1126/science.1219631
87. Iess, L., Rappaport, N.J., Jacobson, R.A., Racioppa, P., Stevenson, D.J., Tortora, P., Armstrong, J.W., Asmar, S.W.: Gravity field, shape, and moment of inertia of Titan. Science **327**(5971), 1367–1369 (2010)
88. Jaccard, C.: MECHANISM OF THE ELECTRICAL CONDUCTIVITY IN ICE. Annals of the New York Academy of Sciences **125**(2), 390–400 (1965). DOI 10.1111/j.1749-6632.1965.tb45405.x
89. Jacobson, R.A., Antreasian, P.G., Bordi, J.J., Criddle, K.E., Ionasescu, R., Jones, J.B., Mackenzie, R.A., Meek, M.C., Parcher, D., Pelletier, F.J., et al.: The gravity field of the saturnian system from satellite observations and spacecraft tracking data. The Astronomical Journal **132**(6), 2520–2526 (2006). DOI 10.1086/508812
90. Journaux, B., Brown, J., Pakhomova, A., Collings, I., Petitgirard, S., Espinoza, P., Boffa Ballaran, T., Vance, S., Ott, J., Cova, F., Garbarino, G., Hanfland, M.: Holistic approach for studying planetary hydrospheres: Gibbs representation of ices thermodynamics, elasticity and the water phase diagram to 2300 mpa. Journal of Geophysical Research Planets (2020). DOI 10.1029/2019JE006176
91. Journaux, B., Caracas, R., Carrez, P., Gouriet, K., Cordier, P., Daniel, I.: Elasticity and dislocations in ice X under pressure. Physics of the Earth and Planetary Interiors **236**, 10–15 (2014). DOI 10.1016/j.pepi.2014.08.002
92. Journaux, B., Daniel, I., Caracas, R., Montagnac, G., Cardon, H.: Influence of NaCl on ice VI and ice VII melting curves up to 6GPa, implications for large icy moons. Icarus **226**(1), 355–363 (2013). DOI 10.1016/j.icarus.2013.05.039
93. Journaux, B., Daniel, I., Petitgirard, S., Cardon, H., Perrillat, J.P., Caracas, R., Mezouar, M.: Salt partitioning between water and high-pressure ices. implication for the dynamics and habitability of icy moons and water-rich planetary bodies. Earth and Planetary Science Letters **463**, 36 – 47 (2017). DOI http://dx.doi.org/10.1016/j.epsl.2017.01.017
94. Jr, E.D.S., Koh, C.: Clathrate Hydrates of Natural Gases, Third Edition. CRC Press (2007). Google-Books-ID: T7LC8ldaVR4C
95. Kalousová, K., Sotin, C., Choblet, G., Tobie, G., Grasset, O.: Two-phase convection in Ganymede's high-pressure ice layer — implications for its geological

evolution. Icarus **299**, 133–147 (2018). DOI 10.1016/j.icarus.2017.07.018
96. Kalousová, K., Sotin, C.: Melting in High-Pressure Ice Layers of Large Ocean Worlds—Implications for Volatiles Transport. Geophysical Research Letters **45**(16), 8096–8103 (2018). DOI 10.1029/2018GL078889
97. Kaltenegger, L., Sasselov, D., Rugheimer, S.: Water-planets in the habitable zone: atmospheric chemistry, observable features, and the case of kepler-62e and-62f. The Astrophysical Journal Letters **775**(2), L47 (2013)
98. Kamata, S., Nimmo, F., Sekine, Y., Kuramoto, K., Noguchi, N., Kimura, J., Tani, A.: Pluto's ocean is capped and insulated by gas hydrates. Nat. Geosci. **12**, 407–410 (2019). DOI 10.1038/s41561-019-0369-8
99. Kelemen, P.B., Hirth, G.: Reaction-driven cracking during retrograde metamorphism: Olivine hydration and carbonation. Earth and Planetary Science Letters **345**, 81–89 (2012)
100. Khurana, K., Kivelson, M., Russell, C., Walker, R., Southwood, D.: Absence of an internal magnetic field at callisto. Nature **387**(6630), 262 (1997)
101. Kimura, J., Nakagawa, T., Kurita, K.: Size and compositional constraints of Ganymede's metallic core for driving an active dynamo. Icarus **202**(1), 216–224 (2009)
102. Kirk, R., Stevenson, D.: Thermal evolution of a differentiated Ganymede and implications for surface features. Icarus **69**(1), 91–134 (1987)
103. Kitzmann, D., Alibert, Y., Godolt, M., Grenfell, J.L., Heng, K., Patzer, A.B.C., Rauer, H., Stracke, B., von Paris, P.: The unstable CO2 feedback cycle on ocean planets. arXiv:1507.01727 [astro-ph] (2015). DOI 10.1093/mnras/stv1487. ArXiv: 1507.01727
104. Kivelson, M., Khurana, K., Volwerk, M.: The permanent and inductive magnetic moments of Ganymede. Icarus **157**(2), 507–522 (2002)
105. Klotz, S., Bove, L., Strässle, T., Hansen, T., Saitta, A.: The preparation and structure of salty ice VII under pressure. Nature Materials **8**, 405–409 (2009)
106. Klotz, S., Komatsu, K., Kagi, H., Kunc, K., Sano-Furukawa, A., Machida, S., Hattori, T.: Bulk moduli and equations of state of ice VII and ice VIII. Physical Review B **95**(17), 174111 (2017). DOI 10.1103/PhysRevB.95.174111
107. Kruijer, T.S., Burkhardt, C., Budde, G., Kleine, T.: Age of jupiter inferred from the distinct genetics and formation times of meteorites. Proceedings of the National Academy of Sciences **114**(26), 6712–6716 (2017)
108. Kuramoto, K., Matsui, T.: Formation of a hot proto-atmosphere on the accreting giant icy satellite: Implications for the origin and evolution of titan, ganymede, and callisto. Journal of Geophysical Research: Planets **99**(E10), 21183–21200 (1994)
109. Kuskov, O.L., Kronrod, V.A.: Core Sizes and Internal Structure of Earth's and Jupiter's Satellites. Icarus **151**, 204–227 (2001). DOI 10.1006/icar.2001.6611
110. Kuskov, O.L., Kronrod, V.A.: Internal structure of Europa and Callisto. Icarus **177**, 550–569 (2005). DOI 10.1016/j.icarus.2005.04.014
111. Larionov, E.G., Kryukov, P.A.: The conductivity of MgSO4 aqueous-solutions in the range of temperatures 298-423K and pressures 0,1-784,6 MPa. Izvestiya Sibirskogo Otdeleniya Akademii Nauk SSSR Seriya Khimicheskikh Nauk (5), 20–23 (1984)
112. Lehmer, O.R., Catling, D.C.: Rocky worlds limited to 1.8 earth radii by atmospheric escape during a star's extreme uv saturation. The Astrophysical Journal **845**(2), 130 (2017)

113. Leitner, M.A., Lunine, J.I.: Modeling early Titan's ocean composition. Icarus **333**, 61–70 (2019)
114. Lemasquerier, D., Grannan, A., Vidal, J., Cébron, D., Favier, B., Le Bars, M., Aurnou, J.: Libration-driven flows in ellipsoidal shells. Journal of Geophysical Research: Planets **122**(9), 1926–1950 (2017)
115. Liu, B., Gao, Y., Han, Y., Ma, Y., Gao, C.: In situ electrical conductivity measurements of H2o under static pressure up to 28 GPa. Physics Letters A **380**(37), 2979–2983 (2016). DOI 10.1016/j.physleta.2016.07.007
116. Liu, C., Mafety, A., Queyroux, J.A., Wilson, C.W., Zhang, H., Béneut, K., Marchand, G.L., Baptiste, B., Dumas, P., Garbarino, G., Finocchi, F., Loveday, J.S., Pietrucci, F., Saitta, A.M., Datchi, F., Ninet, S.: Topologically frustrated ionisation in a water-ammonia ice mixture. Nature Communications **8**(1), 1065 (2017). DOI 10.1038/s41467-017-01132-z
117. Léger, A., Selsis, F., Sotin, C., Guillot, T., Despois, D., Mawet, D., Ollivier, M., Labèque, A., Valette, C., Brachet, F.: A new family of planets? Icarus **169**(2), 499–504 (2004)
118. Malhotra, R.: Tidal origin of the Laplace resonance and the resurfacing of Ganymede. Icarus **94**, 399–412 (1991). DOI 10.1016/0019-1035(91)90237-N
119. Mantegazzi, D., Sanchez-Valle, C., Driesner, T.: Thermodynamic properties of aqueous NaCl solutions to 1073k and 4.5gpa, and implications for dehydration reactions in subducting slabs. Geochimica et Cosmochimica Acta **121**, 263–290 (2013). DOI 10.1016/j.gca.2013.07.015
120. Marounina, N., Grasset, O., Tobie, G., Carpy, S.: Role of the global water ocean on the evolution of Titan's primitive atmosphere. Icarus **310**, 127–139 (2018). DOI 10.1016/j.icarus.2017.10.048
121. Massani, B., Mitterdorfer, C., Loerting, T.: Formation and decomposition of CO2-filled ice. The Journal of Chemical Physics **147**(13), 134503 (2017). DOI 10.1063/1.4996270
122. McKay, C.P., Scattergood, T.W., Pollack, J.B., Borucki, W.J., Van Ghyseghem, H.T.: High-temperature shock formation of $N_2$ and organics on primordial Titan. Nature **332**(6164), 520 (1988)
123. McKinnon, W.: Core evolution in the icy galilean satellites, and the prospects for dynamo-generated magnetic fields. In: Bulletin of the American Astronomical Society, vol. 28, p. 1076 (1996)
124. McKinnon, W.B.: On convection in ice I shells of outer Solar System bodies, with detailed application to Callisto. Icarus **183**(2), 435–450 (2006). DOI 10.1016/j.icarus.2006.03.004
125. Miller, K.E., Glein, C.R., Waite, J.H.: Contributions from accreted organics to Titan's atmosphere: New insights from cometary and chondritic data. The Astrophysical Journal **871**(1), 59 (2019). DOI 10.3847/1538-4357/aaf561
126. Millot, M., Coppari, F., Rygg, J.R., Barrios, A.C., Hamel, S., Swift, D.C., Eggert, J.H.: Nanosecond X-ray diffraction of shock-compressed superionic water ice. Nature **569**(7755), 251 (2019). DOI 10.1038/s41586-019-1114-6
127. Millot, M., Hamel, S., Rygg, J.R., Celliers, P.M., Collins, G.W., Coppari, F., Fratanduono, D.E., Jeanloz, R., Swift, D.C., Eggert, J.H.: Experimental evidence for superionic water ice using shock compression. Nature Physics p. 1 (2018). DOI 10.1038/s41567-017-0017-4
128. Mitri, G., Meriggiola, R., Hayes, A., Lefevre, A., Tobie, G., Genova, A., Lunine, J.I., Zebker, H.: Shape, topography, gravity anomalies and tidal deformation of

Titan. Icarus **236**, 169–177 (2014). DOI 10.1016/j.icarus.2014.03.018
129. Monteux, J., Tobie, G., Choblet, G., Le Feuvre, M.: Can large icy moons accrete undifferentiated? Icarus **237**, 377–387 (2014). DOI 10.1016/j.icarus.2014.04.041
130. Morard, G., Andrault, D., Guignot, N., Sanloup, C., Mezouar, M., Petitgirard, S., Fiquet, G.: In situ determination of fe–$fe_3s$ phase diagram and liquid structural properties up to 65 gpa. Earth and Planetary Science Letters **272**(3), 620–626 (2008)
131. Morard, G., Sanloup, C., Fiquet, G., Mezouar, M., Rey, N., Poloni, R., Beck, P.: Structure of eutectic fe–fes melts to pressures up to 17 gpa: implications for planetary cores. Earth and Planetary Science Letters **263**(1), 128–139 (2007)
132. Mosqueira, I., Estrada, P.R.: Formation of the regular satellites of giant planets in an extended gaseous nebula I: subnebula model and accretion of satellites. Icarus **163**, 198–231 (2003). DOI 10.1016/S0019-1035(03)00076-9
133. Mosqueira, I., Estrada, P.R.: Formation of the regular satellites of giant planets in an extended gaseous nebula II: satellite migration and survival. Icarus **163**, 232–255 (2003). DOI 10.1016/S0019-1035(03)00077-0
134. Nagel, K., Breuer, D., Spohn, T.: A model for the interior structure, evolution, and differentiation of Callisto. Icarus **169**, 402–412 (2004). DOI 10.1016/j.icarus.2003.12.019
135. Nakamura, R., Ohtani, E.: The high-pressure phase relation of the MgSO4–H2o system and its implication for the internal structure of Ganymede. Icarus **211**(1), 648–654 (2011). DOI 10.1016/j.icarus.2010.08.029
136. Néri, A., Guyot, F., Reynard, B., Sotin, C.: A carbonaceous chondrite and cometary origin for icy moons of Jupiter and Saturn. Earth and Planetary Science Letters p. 115920 (2019). DOI 10.1016/j.epsl.2019.115920
137. Nettelmann, N., Helled, R., Fortney, J., Redmer, R.: New indication for a dichotomy in the interior structure of Uranus and Neptune from the application of modified shape and rotation data. Planetary and Space Science (2012)
138. Niemann, H.B., Atreya, S.K., Bauer, S.J., Carignan, G.R., Demick, J.E., Frost, R.L., Gautier, D., Haberman, J.A., Harpold, D.N., Hunten, D.M., Israel, G., Lunine, J.I., Kasprzak, W.T., Owen, T.C., Paulkovich, M., Raulin, F., Raaen, E., Way, S.H.: The abundances of constituents of Titan's atmosphere from the GCMS instrument on the Huygens probe. NATURE **438**(7069), 779–784 (2005)
139. Noack, L., Höning, D., Rivoldini, A., Heistracher, C., Zimov, N., Journaux, B., Lammer, H., Van Hoolst, T., Bredehöft, J.: Water-rich planets: How habitable is a water layer deeper than on earth? Icarus **277**, 215–236 (2016)
140. Noack, L., Snellen, I., Rauer, H.: Water in Extrasolar Planets and Implications for Habitability. Space Science Reviews **212**(1-2), 877–898 (2017). DOI 10.1007/s11214-017-0413-1
141. Néri, A., Guyot, F., Reynard, B., Sotin, C.: A carbonaceous chondrite and cometary origin for icy moons of Jupiter and Saturn. Earth and Planetary Science Letters p. 115920 (2019). DOI 10.1016/j.epsl.2019.115920
142. Ogihara, M., Ida, S.: N-body simulations of satellite formation around giant planets: origin of orbital configuration of the galilean moons. The Astrophysical Journal **753**(1), 60 (2012)
143. Okada, T., Iitaka, T., Yagi, T., Aoki, K.: Electrical conductivity of ice VII. Scientific Reports **4** (2014). DOI 10.1038/srep05778
144. O'Rourke, J.G., Stevenson, D.J.: Stability of ice/rock mixtures with application to a partially differentiated Titan. Icarus **227**, 67–77 (2014). DOI

10.1016/j.icarus.2013.09.010
145. Palumbo, M.E.: The morphology of interstellar water ice. In: Journal of Physics: Conference Series, vol. 6, p. 211. IOP Publishing (2005)
146. Pommier, A., Laurenz, V., Davies, C.J., Frost, D.J.: Melting phase relations in the fe-s and fe-so systems at core conditions in small terrestrial bodies. Icarus **306**, 150–162 (2018)
147. Postberg, F., Khawaja, N., Abel, B., Choblet, G., Glein, C.R., Gudipati, M.S., Henderson, B.L., Hsu, H.W., Kempf, S., Klenner, F., Moragas-Klostermeyer, G., Magee, B., Nölle, L., Perry, M., Reviol, R., Schmidt, J., Srama, R., Stolz, F., Tobie, G., Trieloff, M., Waite, J.H.: Macromolecular organic compounds from the depths of Enceladus. Nature **558**(7711), 564 (2018). DOI 10.1038/s41586-018-0246-4
148. Robinson, V.N., Wang, Y., Ma, Y., Hermann, A.: Stabilization of ammonia-rich hydrate inside icy planets. Proceedings of the National Academy of Sciences **114**(34), 9003–9008 (2017). DOI 10.1073/pnas.1706244114
149. Ronnet, T., Mousis, O., Vernazza, P.: Pebble Accretion at the Origin of Water in Europa. Astropys. J. **845**, 92 (2017). DOI 10.3847/1538-4357/aa80e6
150. Rosso, L.d., Celli, M., Ulivi, L.: New porous water ice metastable at atmospheric pressure obtained by emptying a hydrogen-filled ice. Nature Communications **7**, 13394 (2016). DOI 10.1038/ncomms13394
151. Rückriemen, T., Breuer, D., Spohn, T.: The fe-snow regime in ganymede's core: A deep-seated dynamo below a stable snow zone. Journal of Geophysical Research: Planets **497**, 365–380 (2015)
152. Russell, M.J., Barge, L.M., Bhartia, R., Bocanegra, D., Bracher, P.J., Branscomb, E., Kidd, R., McGlynn, S., Meier, D.H., Nitschke, W., Shibuya, T., Vance, S., White, L., Kanik, I.: The drive to life on wet and icy worlds. Astrobiology **14**(4), 308–343 (2014). DOI 10.1089/ast.2013.1110
153. Rückriemen, T., Breuer, D., Spohn, T.: Top-down freezing in a fe-fes core and ganymede's present-day magnetic field. Icarus **307**, 172 – 196 (2018)
154. Sasaki, T., Stewart, G.R., Ida, S.: Origin of the Different Architectures of the Jovian and Saturnian Satellite Systems. ApJ **714**, 1052–1064 (2010). DOI 10.1088/0004-637X/714/2/1052
155. Schubert, G., Anderson, J., Spohn, T., McKinnon, W.: Interior composition, structure and dynamics of the Galilean satellites. Jupiter: The Planet, Satellites and Magnetosphere pp. 281–306 (2004)
156. Schubert, G., Spohn, T., Reynolds, R.T.: Thermal histories, compositions and internal structures of the moons of the solar system. In: IAU Colloq. 77: Some Background about Satellites, pp. 224–292 (1986)
157. Scott, H., Williams, Q., Ryerson, F.: Experimental constraints on the chemical evolution of large icy satellites. Earth and Planetary Science Letters **203**(1), 399–412 (2002)
158. Sekine, Y., Genda, H., Sugita, S., Kadono, T., Matsui, T.: Replacement and late formation of atmospheric n2 on undifferentiated titan by impacts. Nature Geoscience **4**(6), 359–362 (2011)
159. Sekine, Y., Shibuya, T., Postberg, F., Hsu, H.W., Suzuki, K., Masaki, Y., Kuwatani, T., Mori, M., Hong, P.K., Yoshizaki, M., Tachibana, S., Sirono, S.: High-temperature water-rock interactions and hydrothermal environments in the chondrite-like core of Enceladus. Nature Comm. **6**, 8604 (2015). DOI 10.1038/ncomms9604

160. Shock, E.L., Holland, M.E.: Quantitative habitability. Astrobiology **7**(6), 839–851 (2007). DOI 10.1089/ast.2007.0137
161. Showman, A., Malhotra, R.: Tidal evolution into the laplace resonance and the resurfacing of ganymede. Icarus **127**(1), 93–111 (1997)
162. Soderlund, K., Heimpel, M., King, E., Aurnou, J.: Turbulent models of ice giant internal dynamics: Dynamos, heat transfer, and zonal flows. Icarus (2013)
163. Sohl, F., Choukroun, M., Kargel, J., Kimura, J., Pappalardo, R., Vance, S., Zolotov, M.: Subsurface Water Oceans on Icy Satellites: Chemical Composition and Exchange Processes. Space Science Reviews **153**, 485–510 (2010). DOI 10.1007/s11214-010-9646-y
164. Sohl, F., Sears, W.D., Lorenz, R.D.: Tidal dissipation on titan. Icarus **115**(2), 278–294 (1995)
165. Sohl, F., Spohn, T., Breuer, D., Nagel, K.: Implications from Galileo observations on the interior structure and chemistry of the Galilean satellites. Icarus **157**(1), 104–119 (2002)
166. Sotin, C., Gillet, P., Poirier, J.: Creep of high-pressure ice vi. In: Ices in the solar system, pp. 109–118. Springer (1985)
167. Sotin, C., Grasset, O.: Mass-radius curve for extrasolar Earth-like planets and ocean planets. Icarus **191**, 337–351 (2007)
168. Sotin, C., Parmentier, E.: On the stability of a fluid layer containing a univariant phase transition: application to planetary interiors. Physics of the Earth and Planetary Interiors **55**(1), 10–25 (1989). DOI 10.1016/0031-9201(89)90229-X
169. Sotin, C., Poirier, J.: Viscosity of ice v. Le Journal de Physique Colloques **48**(C1), 1–1 (1987)
170. Spohn, T., Breuer, D.: Interior structure and evolution of the galilean satellites. In: Planetary Systems: The Long View, p. 135 (1998)
171. Squyres, S.W., Reynolds, R.T., Summers, A.L., Shung, F.: Accretional heating of the satellites of Saturn and Uranus. J. Geophys. Res. **93**, 8779–8794 (1988). DOI 10.1029/JB093iB08p08779
172. Stähler, S.C., Panning, M.P., Vance, S.D., Lorenz, R.D., van Driel, M., Nissen-Meyer, T., Kedar, S.: Seismic wave propagation in icy ocean worlds. Journal of Geophysical Research: Planets **123**(1), 206–232 (2018)
173. Stevenson, D.J., Spohn, T., Schubert, G.: Magnetism and thermal evolution of the terrestrial planets. Icarus **54**(3), 466–489 (1983)
174. Tammann, G.: Ueber die Grenzen des festen Zustandes IV. Annalen der Physik **307**(5), 1–31 (1900). DOI 10.1002/andp.19003070502
175. Tobie, G., Gautier, D., Hersant, F.: Titan's bulk composition constrained by cassini-huygens: Implication for internal outgassing. The Astrophysical Journal **752**(2), 125 (2012)
176. Tobie, G., Grasset, O., Lunine, J.I., Mocquet, A., Sotin, C.: Titan's internal structure inferred from a coupled thermal-orbital model. Icarus **175**(2), 496–502 (2005)
177. Tobie, G., Lunine, J., Sotin, C.: Episodic outgassing as the origin of atmospheric methane on Titan. Nature **440**(7080), 61–4 (2006)
178. Tobie, G., Lunine, J.I., Monteux, J., Mousis, O., Nimmo, F.: The origin and evolution of Titan, p. 29 (2014)
179. Tobie, G., Mocquet, A., Sotin, C.: Tidal dissipation within large icy satellites: Applications to Europa and Titan. Icarus **177**, 534–549 (2005). DOI 10.1016/j.icarus.2005.04.006

180. Turtle, E., Barnes, J., Trainer, M., Lorenz, R., MacKenzie, S., Hibbard, K.: Exploring Titan's prebiotic organic chemistry and habitability. LPI Contributions p. 1958 (2017)
181. Valenti, P., Bodnar, R.J., Schmidt, C.: Experimental determination of H2o–NaCl liquidi to 25mass% NaCl and 1.4gpa: Application to the Jovian satellite Europa. Geochimica et Cosmochimica Acta **92**(C), 117–128 (2012). DOI 10.1016/j.gca.2012.06.007
182. Vance, S., Bouffard, M., Choukroun, M., Sotin, C.: Ganymede's internal structure including thermodynamics of magnesium sulfate oceans in contact with ice. Planetary And Space Science **96**, 62–70 (2014)
183. Vance, S., Bouffard, M., Choukroun, M., Sotin, C.: Ganymedes internal structure including thermodynamics of magnesium sulfate oceans in contact with ice. Planetary and Space Science **96**, 62–70 (2014). DOI 10.1016/j.pss.2014.03.011
184. Vance, S., Brown, J.M.: Thermodynamic properties of aqueous MgSO4 to 800 MPa at temperatures from - 20 to 100 C and concentrations to 2.5mol kg-1 from sound speeds, with applications to icy world oceans. Geochimica et Cosmochimica Acta **110**, 176–189 (2013). DOI 10.1016/j.gca.2013.01.040
185. Vance, S., Harnmeijer, J., Kimura, J., Hussmann, H., deMartin, B., Brown, J.M.: Hydrothermal systems in small ocean planets. Astrobiology **7**(6), 987–1005 (2007). DOI 10.1089/ast.2007.0075
186. Vance, S.D., Hand, K.P., Pappalardo, R.T.: Geophysical controls of chemical disequilibria in Europa. Geophysical Research Letters **43**(10), 4871–4879 (2016). DOI 10.1002/2016gl068547
187. Vance, S.D., Panning, M.P., Stähler, S., Cammarano, F., Bills, B.G., Tobie, G., Kamata, S., Kedar, S., Sotin, C., Pike, W.T., et al.: Geophysical investigations of habitability in ice-covered ocean worlds. Journal of Geophysical Research: Planets (2018). DOI 10.1002/2017je005341
188. Vance, S.D., Panning, M.P., Stähler, S., Cammarano, F., Bills, B.G., Tobie, G., Kamata, S., Kedar, S., Sotin, C., Pike, W.T., Lorenz, R., Huang, H.H., Jackson, J.M., Banerdt, B.: Geophysical Investigations of Habitability in Ice-Covered Ocean Worlds: GEOPHYSICAL HABITABILITY. Journal of Geophysical Research: Planets **123**(1), 180–205 (2018). DOI 10.1002/2017JE005341
189. Wagner, W., Pruß, A.: The IAPWS formulation 1995 for the thermodynamic properties of ordinary water substance for general and scientific use. Journal of Physical and Chemical Reference Data **31**(2), 387–535 (2002)
190. Wagner, W., Riethmann, T., Feistel, R., Harvey, A.H.: New equations for the sublimation pressure and melting pressure of h2o ice ih. Journal of Physical and Chemical Reference Data **40**(4), 043103 (2011)
191. Wagner, W., Riethmann, T., Feistel, R., Harvey, A.H.: New Equations for the Sublimation Pressure and Melting Pressure of H2o Ice Ih. Journal of Physical and Chemical Reference Data **40**(4), 043103 (2011). DOI 10.1063/1.3657937
192. Waite, W.F., Stern, L.A., Kirby, S.H., Winters, W.J., Mason, D.H.: Simultaneous determination of thermal conductivity, thermal diffusivity and specific heat in sI methane hydrate. Geophysical Journal International **169**(2), 767–774 (2007). DOI 10.1111/j.1365-246X.2007.03382.x
193. Wang, H., Zeuschner, J., Eremets, M., Troyan, I., Willams, J.: Stable solid and aqueous $H_2CO_3$ from $CO_2$ and $H_2O$ at high pressure and high temperature. Scientific Reports **6**, 19902 (2016). DOI 10.1038/srep19902

194. Williams, Q.: Bottom-up versus top-down solidification of the cores of small solar system bodies: Constraints on paradoxical cores. Earth and Planetary Science Letters **284**(3), 564–569 (2009)
195. Yoshino, T., Walter, M.J., Katsura, T.: Core formation in planetesimals triggered by permeable flow. Nature **422**(6928), 154 (2003)
196. Zhan, X., Schubert, G.: Powering ganymede's dynamo. Journal of Geophysical Research **117**(E8), E08011 (2012)
197. Zolotov, M.Y.: Oceanic Composition on Europa: Constraints from Mineral Solubilities. Lunar and Planetary Institute Science Conference Abstracts **39**, 2349 (2008)